

Piezomagnetic fields associated with a dislocation source in a layered elastic medium

Ken'ichi Yamazaki 

Miyazaki Observatory, Disaster Prevention Research Institute, Kyoto University, 3884 Kaeda, Miyazaki 889-2161, Japan. E-mail:

kenichi@rcep.dpri.kyoto-u.ac.jp

Accepted 2021 April 16. Received 2021 March 21; in original form 2021 February 5

SUMMARY

The piezomagnetic effect is defined as a change in magnetization with applied stress. Changes in the geomagnetic field caused by the piezomagnetic effect, referred to as the piezomagnetic field, have been theoretically estimated and compared by previous studies to interpret observed variations in the geomagnetic field. However, the piezomagnetic field estimated in previous studies may not provide an accurate estimation because they ignored spatial variations in elasticity, leading to only a rough approximation of the properties of Earth's crust. In this paper, a semi-analytical procedure for calculating the piezomagnetic field arising from a point dislocation source embedded in a layered elastic medium is derived. Following a well-established method of the vector surface harmonic expansion, all of the governing equations written in partial differential equations in a real domain, together with the linear constitutive law of the piezomagnetic effect, are converted to a set of ordinary differential equations in a wavenumber domain. Equations in the wavenumber domain are solved analytically, and each component of the piezomagnetic field in the real domain is obtained after applying the Hankel transform. By using the derived procedure, the piezomagnetic and displacement fields due to a finite fault with strike-slip, dip-slip, and tensile-opening mechanisms are estimated for media with layered elasticity structures. Results for a finite fault are obtained by integrating the point source solution over the fault plane. The results of the numerical analysis allow the effect of heterogeneities in rigidity on the piezomagnetic effect to be examined and implications for the findings of previous investigations to be drawn. In cases where the moment-release at the dislocation source is fixed, the effect of the rigidity differences between upper and lower layers on the piezomagnetic field is minor even in the case where the Curie point depth is near the source of dislocation. This result is in contrast to a previous study that assumed the Mogi model and suggested that heterogeneities in the horizontal direction may be of importance when combined with layered rigidity structures. A contrast is seen between the piezomagnetic and displacement fields corresponding to models with layered rigidity structures: the piezomagnetic field is roughly proportional to the moment-release on a source fault, whereas the displacement field is proportional to slip or opening of the fault. Provided that the rigidity of the crust increases with increasing depth, the calculated piezomagnetic field is likely to have been underestimated in many earlier studies, which assumed uniform rigidity and a geodetically inverted size of slip.

Key words: Elasticity and anelasticity; Magnetic properties; Electromagnetic theory; Magnetic anomalies: modelling and interpretation; Rock and mineral magnetism; Mechanics, theory, and modelling.

1 INTRODUCTION

One of the key mechanisms that accounts for changes in the geomagnetic field in association with mechanical activity in Earth's crust is the piezomagnetic effect. The piezomagnetic effect is defined as a change in magnetization with applied stress and has been confirmed by laboratory experiments (e.g. Ohnaka & Kinoshita 1968; Nagata 1970; Pozzi 1977; Zlotnicki *et al.* 1981). Mechanical processes in Earth's crust, including plate collision, earthquake faulting, and pressurization/depressurization of magma, generate changes in stress and consequent

changes in magnetization by means of the piezomagnetic effect, which in turn yields changes in the magnetic field, referred to as the piezomagnetic field. Because the piezomagnetic effect relates observable changes in the geomagnetic field to unobservable changes in the subsurface stress field, studies of the piezomagnetic field have been a topic of interest in geophysics as a tool for monitoring stress states in the crust (e.g. Sasai 1994; Johnston 1997; Uyeshima 2007).

An important subject related to the piezomagnetic field is the methodology used to calculate the expected piezomagnetic field corresponding to a variety of dislocation sources. Generally, to identify the origin of changes in the geomagnetic field in association with crustal activity, observed changes in the magnetic field are compared with values predicted by theory. The origin of the observed changes in the geomagnetic field is identified to be the piezomagnetic effect when the observed and predicted changes in the magnetic field are consistent, as exemplified by cases for earthquakes (Johnston & Mueller 1987; Johnston *et al.* 1994, 2006; Yamazaki 2013) and volcanic activity (e.g. Sasai & Ishikawa 1991; Sasai *et al.* 2002; Del Negro & Currenti 2003; Del Negro *et al.* 2004; Currenti *et al.* 2007). Conversely, the distribution of observed changes in the geomagnetic field is used to constrain the sizes and locations of possible dislocation sources by assuming that the piezomagnetic effect is the major mechanism generating the observed changes in the geomagnetic field (e.g. Sasai & Ishikawa 1980; Del Negro *et al.* 2004; Ueda *et al.* 2006; Napoli *et al.* 2008). Theoretical calculations have also been performed to predict expected changes in the geomagnetic field during future events and to design strategies for observing them (e.g. Shamsi & Stacey 1969; Oshiman *et al.* 1991; Stuart *et al.* 1995; Okubo & Kanda 2010; Yamazaki 2013).

A procedure for numerically calculating the piezomagnetic field is simple in principle (Stacey 1964; Zlotnicki and Cornet 1986): first, the stress field corresponding to assumed dislocation sources in terms of the elastic theory should be calculated, then the distribution of changes in magnetization in terms of the piezomagnetic effect should be determined, and finally the corresponding changes in the magnetic field can be determined. The numerical procedure is applicable to an arbitrary structure of Earth's crust involving heterogeneities of magnetization, elasticity, and topography (e.g. Currenti *et al.* 2009), but it requires long computation times in integral calculation to obtain a precise result.

Analytical expressions of the piezomagnetic field are useful for systematically exploring the basic properties of the piezomagnetic field, including its spatial patterns, maximum amplitude, and dependence on dislocation source parameters. With assumptions of uniform magnetization and uniform elasticity, the procedure for calculating the piezomagnetic field is simplified by using Green's theorem (Sasai, 1983, 1986), which enables us to obtain a set of analytical formulae representing the piezomagnetic field corresponding to surface loading (Sasai 1991a), expansion of spherical bodies (Sasai 1991b), and slips and openings on rectangular faults (Sasai 1991a, Utsugi *et al.* 2000). Analytical formulae are used to estimate, based on theoretical considerations, spatial patterns of the piezomagnetic field for a variety of dislocation sources (e.g. Sasai 1991a).

However, many of the analytical formulae may provide an imprecise estimation of the piezomagnetic field because they assume that both magnetization and elasticity are uniform, which gives only a rough approximation of Earth's crust. Concerning the heterogeneity of magnetization, Oshiman (1990) demonstrated by using a two-dimensional simulator that the piezomagnetic field is considerably enhanced when the magnetization is horizontally inhomogeneous. Concerning the heterogeneity of elasticity, Okubo & Oshiman (2004) showed by using a semi-analytical formula for an expansion source in a layered medium that the expected piezomagnetic field depends strongly on the structure of elasticity. For more realistic situations, Currenti *et al.* (2009) concluded that a model with uniform magnetization and uniform elasticity overestimated the expected magnetic changes in the case of the Mount Etna volcano. These results imply that many earlier conclusions regarding the piezomagnetic effect calculated through analytical formulae may be inaccurate, which provides motivation to refine solutions that incorporate heterogeneities in magnetization and/or in elasticity.

In this work, a semi-analytical procedure for determining the piezomagnetic field generated by a point dislocation (i.e. slip or opening) source in a layered elastic medium is presented to assess the validity of previous studies in which uniform elasticity was assumed. In the proposed procedure, the piezomagnetic field is given in the wavenumber domain, and values of the piezomagnetic field in the real domain are obtained after applying the Hankel transform. The same problem has been solved previously only for an expansion source (Okubo & Oshiman 2004), in which the stress field was determined analytically but the magnetic field was determined numerically. In contrast, this paper presents a generalized procedure: both the stress and magnetic fields are determined analytically, and dislocation sources are dealt with as well as expansion sources. The possibility of this extension was mentioned by Currenti *et al.* (2008), but the explicit procedure has not been presented so far.

The remainder of this paper is organized as follows. In Section 2, the governing equations are presented. In Section 3, the configuration of the medium is defined together with boundary conditions, and a set of analytic solutions for the displacement, magnetization, and piezomagnetic fields is derived in a wavenumber domain. A key point in deriving the solution is how to express the constitutive law of the linear piezomagnetic effect (e.g. Sasai 1991a) in the wavenumber domain. In Section 4, some numerical examples obtained by the derived formula are presented, and qualitative discussion on the effect of elastic boundaries on the piezomagnetic and displacement fields is given. Section 5 contains the main conclusions of the study.

2 GOVERNING EQUATIONS

In calculating the piezomagnetic field, the displacement–stress field, changes in magnetization, and changes in the magnetic field should be considered simultaneously. A cylindrical set of coordinates (r, ϕ, z) is adopted. All vectors are expressed in the form of

$$\xi(r, \phi, z) = \xi_r(r, \phi, z)\mathbf{e}_r + \xi_\phi(r, \phi, z)\mathbf{e}_\phi + \xi_z(r, \phi, z)\mathbf{e}_z, \quad (1)$$

where ξ_i ($i = r, \phi, z$) can be u_i , τ_{zi} , m_i , B_i and H_i , which are defined below, and \mathbf{e}_r , \mathbf{e}_ϕ and \mathbf{e}_z are basis vectors in each direction in the cylindrical coordinate system.

The displacement–stress field is determined by equilibrium equations and a constitutive law relating derivatives of the displacement and stress fields. Except for the source level at which the dislocation exists, the equilibrium equation is given by

$$\partial_z \tau_{rz} + \partial_r \tau_{rr} + r^{-1} \partial_\phi \tau_{r\phi} + r^{-1} (\tau_{rr} - \tau_{\phi\phi}) = 0, \quad (2)$$

$$\partial_z \tau_{\phi z} + \partial_r \tau_{r\phi} + r^{-1} \partial_\phi \tau_{\phi\phi} + 2r^{-1} \tau_{r\phi} = 0, \quad (3)$$

$$\partial_z \tau_{zz} + \partial_r \tau_{rz} + r^{-1} \partial_\phi \tau_{\phi z} + r^{-1} \tau_{rz} = 0, \quad (4)$$

where u_j and τ_{ij} ($i = r, \phi, z$) are the displacement vector and the stress tensor, respectively. The displacement and stress fields are assumed to be related to Hooke's law for an isotropic medium:

$$\tau_{rr} = (\lambda + 2G) \partial_r u_r + \lambda (\partial_z u_z + r^{-1} \partial_\phi u_\phi + r^{-1} u_r), \quad (5)$$

$$\tau_{\phi\phi} = (\lambda + 2G) r^{-1} (\partial_\phi u_\phi + u_r) + \lambda (\partial_z u_z + \partial_r u_r), \quad (6)$$

$$\tau_{zz} = (\lambda + 2G) \partial_z u_z + \lambda (\partial_r u_r + r^{-1} \partial_\phi u_\phi + r^{-1} u_r), \quad (7)$$

$$\tau_{rz} = G (\partial_z u_r + \partial_r u_z), \quad (8)$$

$$\tau_{\phi z} = G (r^{-1} \partial_\phi u_z + \partial_z u_\phi), \quad (9)$$

$$\tau_{r\phi} = G (\partial_r u_\phi - r^{-1} u_\phi + r^{-1} \partial_\phi u_r), \quad (10)$$

where λ and G are Lamé's first constant and shear modulus, respectively.

Changes in magnetization, m_i ($i = r, \phi, z$), are related to changes in stress in terms of the constitutive law of the piezomagnetic effect. The constitutive law is given by (Sasai 1991a):

$$m_i = \frac{3}{2} \beta (T_{ir} M_r + T_{i\phi} M_\phi + T_{iz} M_z), \quad (11)$$

where

$$T_{ij} \equiv \tau_{ij} - \delta_{ij} T, \quad (12)$$

$$T = \frac{1}{3} (\tau_{rr} + \tau_{\phi\phi} + \tau_{zz}), \quad (13)$$

where β is the stress sensitivity of the piezomagnetic effect, M_i is the initial magnetization of the medium and δ_{ij} is the Kronecker delta. However, this form is somewhat inconvenient in the cylindrical coordinate system because M_r and M_ϕ depend on ϕ even when the direction of the magnetization is constant. To rewrite the expression, the relationship between the horizontal components of a vector in the Cartesian and cylindrical coordinates is used:

$$M_r = M_x \cos \phi + M_y \sin \phi, \quad (14)$$

$$M_\phi = -M_x \sin \phi + M_y \cos \phi. \quad (15)$$

Using this relationship and the definition of T_{ij} (eq. 12), the constitutive law of the piezomagnetic effect (eq. 11) is rewritten as

$$\frac{2}{3\beta} m_r = M_{-1} (\tau_{rr} + i \tau_{r\phi} - T) e^{i\phi} + M_{+1} (\tau_{rr} - i \tau_{r\phi} - T) e^{-i\phi} + M_z \tau_{rz}, \quad (16)$$

$$\frac{2}{3\beta} m_\phi = M_{-1} (\tau_{\phi r} + i \tau_{\phi\phi} - iT) e^{i\phi} + M_{+1} (\tau_{\phi r} - i \tau_{\phi\phi} + iT) e^{-i\phi} + M_z \tau_{\phi z}, \quad (17)$$

$$\frac{2}{3\beta} m_z = M_{-1} (\tau_{zr} + i \tau_{z\phi}) e^{i\phi} + M_{+1} (\tau_{zr} - i \tau_{z\phi}) e^{-i\phi} + M_z (\tau_{zz} - T), \quad (18)$$

where $M_{\pm 1} = (M_x \pm i M_y)/2$. Because M_{+1} and M_{-1} are constants within a volume in which the magnetization vector is constant, these expressions (eqs 16–18) are more useful in the cylindrical coordinate system than is the original expression (eq. 11) and are thus used in the following analysis.

Changes in the magnetic field obey the equations

$$\nabla \times \mathbf{H} = \mathbf{0}, \quad (19)$$

$$\nabla \cdot \mathbf{B} = 0, \quad (20)$$

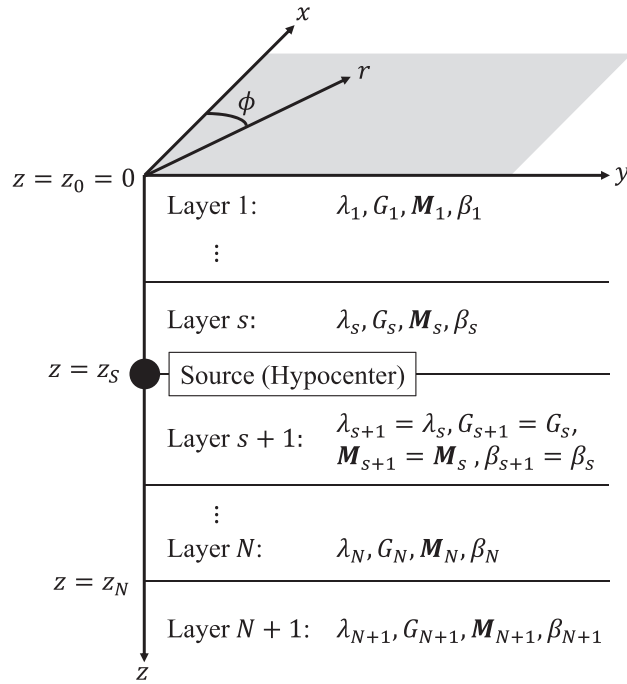


Figure 1. General form of the layered model for which solutions of the displacement–stress and magnetic fields are derived. Note that both of the elastic constants (λ and G) and magnetic properties (\mathbf{M} and β) are treated as layer boundaries. The magnetization of the bottom layer is always zero because this layer is below the Curie point depth.

where \mathbf{H} and \mathbf{B} are changes in the magnetic field and magnetic induction, respectively, and are related to changes in magnetization as

$$\mathbf{B} = \mu_0 (\mathbf{H} + \mathbf{m}), \quad (21)$$

where μ_0 is the magnetic permeability in the vacuum whose value in SI units is $4\pi \times 10^{-7} \text{ Hm}^{-1}$. In the cylindrical coordinate system, each component of eq. (19) is given by

$$r^{-1} \partial_\phi H_z - \partial_z H_\phi = 0, \quad (22)$$

$$\partial_z H_r - \partial_r H_z = 0, \quad (23)$$

$$\partial_r (r H_\phi) - \partial_\phi H_r = 0, \quad (24)$$

eq. (20) is given by

$$r^{-1} \partial_r (r B_r) + r^{-1} \partial_\phi B_\phi + \partial_z B_z = 0, \quad (25)$$

and eq. (21) is given by

$$B_i = \mu_0 (H_i + m_i). \quad (i = r, \phi, z) \quad (26)$$

Note that the problem is semi-coupled: changes in stress cause changes in magnetization, and changes in magnetization cause changes in the magnetic field, but changes in the reverse order are not induced. Therefore, each problem can be solved successively, namely, the determinations of the stress field, the distribution of magnetization and the magnetic field.

3 SOLUTION OF THE PROBLEM

The displacement–stress and magnetic fields in a layered model were considered in 3-D, as illustrated in Fig. 1. Properties of the medium (i.e. Lamé's first constant, shear modulus, and initial magnetization vector) are uniform in each layer.

3.1 Vector surface harmonic expansion

The vector surface harmonic expansion (Takeuchi & Saito 1972; Kennett & Kerry 1979), which is also referred to as the 'cylindrical system of vector function' (e.g. Pan 1989), but with a different convention of notation, is used to solve the set of governing equations. As preparation,

the divergence and vorticity in the horizontal components ξ_r and ξ_ϕ are introduced as

$$\xi_V(r, \phi) = r^{-1} [\partial_r (r \xi_r(r, \phi)) + \partial_\phi \xi_\phi(r, \phi)], \quad (27)$$

$$\xi_H(r, \phi) = r^{-1} [\partial_r (r \xi_\phi(r, \phi)) - \partial_\phi \xi_r(r, \phi)]. \quad (28)$$

By considering ξ_V and ξ_H instead of ξ_r and ξ_ϕ , many of the governing equations are rewritten to forms in which ∂_r and ∂_ϕ appear only in an operator ∇_h^2 defined by

$$\nabla_h^2 f \equiv r^{-1} \partial_r (r \partial_r f) + r^{-2} \partial_\phi^2 f. \quad (29)$$

the Hankel–Fourier transforms of an arbitrary function $f(r, \phi)$ including ξ_V , ξ_H or ξ_z in the real domain are considered to be defined by

$$\hat{f}(k, m) \equiv \frac{1}{2\pi} \int_0^{2\pi} d\phi e^{-im\phi} \int_0^\infty f(r, \phi) J_m(kr) r dr. \quad (30)$$

where J_m is the m th-order Bessel function of the first kind. Hereinafter, the hat symbol represents the function in the wavenumber domain defined by this transform. After applying the Hankel–Fourier transform, the operator ∇_h^2 is reduced to a scalar multiplier by the formula

$$\frac{1}{2\pi} \int_0^{2\pi} d\phi e^{-im\phi} \int_0^\infty r dr J_m(kr) \nabla_h^2 f(r, \phi) = -k^2 \hat{f}(k, m). \quad (31)$$

The vector surface harmonic expansion for an arbitrary vector value function $\xi(r, \phi, z)$ is

$$\xi(r, \phi, z) = \sum_m \int_0^\infty k dk \left[\hat{\mathcal{U}}(k, m, z) \mathbf{R}_m + \hat{\mathcal{V}}(k, m, z) \mathbf{S}_m + \hat{\mathcal{W}}(k, m, z) \mathbf{T}_m \right], \quad (32)$$

where

$$\mathbf{R}_m = +J_m(kr) e^{im\phi} \mathbf{e}_z, \quad (33)$$

$$\mathbf{S}_m = +\frac{\partial}{\partial(kr)} J_m(kr) e^{im\phi} \mathbf{e}_r + \frac{im}{kr} J_m(kr) e^{im\phi} \mathbf{e}_\phi, \quad (34)$$

$$\mathbf{T}_m = +\frac{im}{kr} J_m(kr) e^{im\phi} \mathbf{e}_r - \frac{\partial}{\partial(kr)} J_m(kr) e^{im\phi} \mathbf{e}_\phi. \quad (35)$$

Eq. (32) is identical to eq. (1) when $\hat{\mathcal{U}}$, $\hat{\mathcal{V}}$ and $\hat{\mathcal{W}}$ are set to

$$\hat{\mathcal{U}} = \hat{\xi}_z, \quad (36)$$

$$\hat{\mathcal{V}} = -k^{-1} \hat{\xi}_V, \quad (37)$$

$$\hat{\mathcal{W}} = k^{-1} \hat{\xi}_H, \quad (38)$$

as directly confirmed by substituting these quantities. Following the definition, components of a vector field ξ_r , ξ_ϕ and ξ_z in the real domain (i.e. functions of r , ϕ and z) are expressed in terms of $\hat{\xi}_V$, $\hat{\xi}_H$ and $\hat{\xi}_z$, which are in the wavenumber domain (i.e. functions of k , m and z), as

$$\xi_r(r, \phi) = \sum_m e^{im\phi} \int_0^\infty k dk \left[-\frac{\partial}{\partial(kr)} J_m(kr) k^{-1} \hat{\xi}_V(k, m) + \frac{im}{kr} J_m(kr) k^{-1} \hat{\xi}_H(k, m) \right], \quad (39)$$

$$\xi_\phi(r, \phi) = \sum_m e^{im\phi} \int_0^\infty k dk \left[-\frac{im}{kr} J_m(kr) k^{-1} \hat{\xi}_V(k, m) - \frac{\partial}{\partial(kr)} J_m(kr) k^{-1} \hat{\xi}_H(k, m) \right], \quad (40)$$

$$\xi_z(r, \phi) = \sum_m e^{im\phi} \int_0^\infty k dk J_m(kr) \hat{\xi}_z(k, m). \quad (41)$$

3.2 Displacement–stress field

The first problem is to determine the displacement–stress field in the considered situation. This is purely an elastic problem, and its solution in a more general situation is found in the literature (e.g. Fukahata & Matsu'ura 2005). However, to relate the solution of the displacement–stress field to the spatial distribution of magnetization in the following subsections and to define the variables used, the derivation of the solution of the displacement–stress field is summarized here.

In each layer, equations for the displacement–stress field (eqs 2–10) are reduced to two sets of ordinary equations after changing variables from ξ_r and ξ_ϕ to ξ_V and ξ_H by eqs (27) and (28), and applying the Hankel–Fourier transformation (eq. 30). In the n th layer, the first set, which involves \hat{u}_z , \hat{u}_V , $\hat{\tau}_{zz}$ and $\hat{\tau}_{Vz}$, is

$$\partial_z \hat{u}_z = -\frac{\lambda_n}{\lambda_n + 2G_n} \hat{u}_V + \frac{1}{\lambda_n + 2G_n} \hat{\tau}_{zz}, \quad (42)$$

$$\partial_z \hat{u}_V = +k^2 \hat{u}_z + \frac{1}{G_n} \hat{\tau}_{Vz}, \quad (43)$$

$$\partial_z \hat{\tau}_{zz} = -\hat{\tau}_{Vz}, \quad (44)$$

$$\partial_z \hat{\tau}_{Vz} = +\frac{4G_n(\lambda_n + G_n)}{\lambda_n + 2G_n} k^2 \hat{u}_V + \frac{\lambda_n}{\lambda_n + 2G_n} k^2 \hat{\tau}_{zz}, \quad (45)$$

and the second set, which involves \hat{u}_H and $\hat{\tau}_{Hz}$, is

$$\partial_z \hat{u}_H = \frac{1}{G_n} \hat{\tau}_{Hz}, \quad (46)$$

$$\partial_z \hat{\tau}_{Hz} = G_n k^2 \hat{u}_H. \quad (47)$$

Parameters with a subscript n represent values in the n th layer.

On the ground surface, each component of the traction vector (i.e. $\hat{\tau}_{Vz}$, $\hat{\tau}_{Hz}$ and $\hat{\tau}_{zz}$) should satisfy

$$\hat{\tau}_{iz}(k, m, z = 0) = 0, \quad (48)$$

when the surface loading is ignored, as is assumed in the present study. In each layer boundary $z = z_n$ ($1 \leq n \leq N$), the dislocation and the traction vector should satisfy the boundary condition in the form of

$$\hat{\chi}_i(k, m, z = z_n + 0) - \hat{\chi}_i(k, m, z = z_n - 0) = \delta_{ns} [\hat{\chi}_i]_s^+(k, m), \quad (49)$$

where $\hat{\chi}_i$ represents \hat{u}_i or $\hat{\tau}_{iz}$, δ_{sn} is the Kronecker delta, s is an integer indicating the source level (see Fig. 1), and $[\hat{\chi}_i]_s^+$ is the discontinuity vector that represents the dislocation source. In addition, both \hat{u}_i and $\hat{\tau}_{iz}$ should be zero at $z \rightarrow \infty$.

Solutions for eqs (42)–(45) and for eqs (46) and (47) are given in the form of

$$\hat{\chi}_i(k, m, z) = \hat{\chi}_{i,+1}^n(k, m) e^{-k(z_n-z)} + \hat{\chi}_{i,+2}^n(k, m) k z e^{-k(z_n-z)} + \hat{\chi}_{i,-1}^n(k, m) e^{-k(z-z_{n-1})} + \hat{\chi}_{i,-2}^n(k, m) k z e^{-k(z-z_{n-1})}. \quad (50)$$

an algebraic procedure for determining $\hat{u}_{i,\alpha}^n(k, m)$ and $\hat{\tau}_{iz,\alpha}^n(k, m)$ ($\alpha = \pm 1, \pm 2$) and their derivations, together with source terms $[\hat{u}_i]_s^+$, $[\hat{\tau}_{iz}]_s^+$, is presented in Appendix A.

3.3 Magnetic field

The next problem is to determine the magnetic field (\mathbf{H} or \mathbf{B}) for a given distribution of magnetization. In general, using a scalar potential Φ , which is defined by $\mathbf{H} = -\nabla\Phi$, is an easier way to determine the magnetic field generated by a given magnetization without temporal variations than directly solving Maxwell's equations. In fact, analytical solutions of the piezomagnetic field in the case of a homogeneous elastic medium have been derived by using the scalar potential (Sasai 1991a; Utsugi *et al.* 2000). However, if the magnetization is not given by m_r , m_ϕ and m_z in the real domain, but by \hat{m}_V , \hat{m}_H (eqs 27 and 28) and \hat{m}_z in the wavenumber domain (eq. 30), the determination of \hat{H}_V , \hat{H}_H and \hat{H}_z followed by the transformation given in eqs (39)–(41) is easier than determining Φ followed by taking its gradient, as derived below.

The same procedure used to determine the displacement–stress field can be applied to determine the magnetic field for a given distribution of magnetization. After transformed to the wavenumber domain, the governing equations (eqs 22–26) are reduced to the following equations for H_i ($i = z, V, H$):

$$\partial_z \hat{H}_V = -k^2 \hat{H}_z, \quad (51)$$

$$\partial_z \hat{H}_z + \hat{H}_V = -\hat{f}, \quad (52)$$

and

$$\hat{H}_H = 0, \quad (53)$$

where

$$\hat{f} = \partial_z \hat{m}_z + \hat{m}_V. \quad (54)$$

As the boundary condition, \hat{H}_V and $\hat{B}_z = \mu_0(\hat{H}_z + \hat{m}_z)$ should be continuous at each boundary. In addition, both \hat{H}_z and \hat{H}_V should be zero at $z \rightarrow \pm\infty$.

Assuming that magnetization is expressed in the form of

$$\hat{m}_i(k, m, z) = \hat{m}_{i,+1}^n(k, m) e^{-k(z_n-z)} + \hat{m}_{i,+2}^n(k, m) k z e^{-k(z_n-z)} + \hat{m}_{i,-1}^n(k, m) e^{-k(z-z_{n-1})} + \hat{m}_{i,-2}^n(k, m) k z e^{-k(z-z_{n-1})}, \quad (55)$$

the solution for eqs (51) and (52) is given in the form of

$$\hat{H}_i(k, m, z) = \hat{H}_{i,+1}^n(k, m) e^{-k(z_n-z)} + \hat{H}_{i,+2}^n(k, m) k z e^{-k(z_n-z)} + \hat{H}_{i,+3}^n(k, m) k^2 z^2 e^{-k(z_n-z)} + \hat{H}_{i,-1}^n(k, m) e^{-k(z-z_{n-1})} + \hat{H}_{i,-2}^n(k, m) k z e^{-k(z-z_{n-1})} + \hat{H}_{i,-3}^n(k, m) k^2 z^2 e^{-k(z-z_{n-1})}. \quad (56)$$

an algebraic procedure to determine $\hat{H}_{i,\alpha}(k, m)$ ($\alpha = \pm 1, \pm 2, \pm 3$) in terms of $\hat{m}_{i,\beta}(k, m)$ ($\beta = \pm 1, \pm 2$) and their derivations are presented in Appendix B.

3.4 Expression of the piezomagnetic constitutive law in the wavenumber domain

The remainder of the problem is to express \hat{m}_i in terms of \hat{u}_i and $\hat{\tau}_{zi}$ ($i = z, V, H$). By instituting the constitutive law of the piezomagnetic effect (eqs 16–18) into the definition of m_V and m_H (eqs 27 and 28), and then using the equilibrium equations (eqs 2–4) and the definition of T (eq. 13), a set of expressions are derived as

$$\frac{2}{3\beta} m_V = M_{-1} [-\partial_z (\tau_{rz} + i\tau_{\phi z}) - (\partial_r + ir^{-1}\partial_\phi) T] e^{i\phi} + M_{+1} [-\partial_z (\tau_{rz} - i\tau_{\phi z}) - (\partial_r - ir^{-1}\partial_\phi) T] e^{-i\phi} + M_z \tau_{zV}, \quad (57)$$

$$\frac{2}{3\beta} m_H = iM_{-1} [\partial_z (\tau_{rz} + i\tau_{\phi z}) - (\partial_r + ir^{-1}\partial_\phi) (\tau_{zz} - 2T)] e^{i\phi} + iM_{+1} [-\partial_z (\tau_{rz} - i\tau_{\phi z}) + (\partial_r - ir^{-1}\partial_\phi) (\tau_{zz} - 2T)] e^{-i\phi} + M_z \tau_{zH}, \quad (58)$$

$$\frac{2}{3\beta} m_z = M_{-1} (\tau_{rz} + i\tau_{\phi z}) e^{i\phi} + M_{+1} (\tau_{rz} - i\tau_{\phi z}) e^{-i\phi} + M_z (\tau_{zz} - T). \quad (59)$$

To transform these expressions into the wavenumber domain, the following formulae are referred to:

$$e^{i\phi} (\partial_r + ir^{-1}\partial_\phi) f(r, \phi) = \sum_m e^{im\phi} \int_0^\infty k dk J_m(kr) [-k \hat{f}(k, m-1)], \quad (60)$$

$$e^{-i\phi} (\partial_r - ir^{-1}\partial_\phi) f(r, \phi) = \sum_m e^{im\phi} \int_0^\infty k dk J_m(kr) [k \hat{f}(k, m+1)], \quad (61)$$

and

$$[\xi_r(r, \phi) + i\xi_\phi(r, \phi)] e^{i\phi} = \sum_m e^{im\phi} \int_0^\infty k dk J_m(kr) [k^{-1} \{\hat{\xi}_V + i\hat{\xi}_H\}(k, m-1)], \quad (62)$$

$$[\xi_r(r, \phi) - i\xi_\phi(r, \phi)] e^{-i\phi} = \sum_m e^{im\phi} \int_0^\infty k dk J_m(kr) [k^{-1} \{-\hat{\xi}_V + i\hat{\xi}_H\}(k, m+1)]. \quad (63)$$

For simplicity of notation, the difference between two functions \hat{f} and \hat{g} with the same set of arguments $\hat{f}(k, m) - \hat{g}(k, m)$ is expressed as $(\hat{f} - \hat{g})(k, m)$ in these formulae. These formulae are based on a recurrence property of the Bessel function $d[x^{\pm m} J_m(x)]/dx = \pm x^{\pm m} J_{m\mp 1}(x)$.

Using eqs (60)–(63), the piezomagnetic constitutive law in the wavenumber domain is expressed as

$$\frac{2}{3\beta} \hat{m}_V(k, m) = M_{-1} [-k^{-1} \partial_z (\hat{\tau}_{Vz} + i\hat{\tau}_{Hz}) + k\hat{T}](k, m-1) + M_{+1} [k^{-1} \partial_z (\hat{\tau}_{Vz} - i\hat{\tau}_{Hz}) - k\hat{T}](k, m+1) + M_z \hat{\tau}_{Vz}(k, m), \quad (64)$$

$$\begin{aligned} \frac{2}{3\beta} \hat{m}_H(k, m) &= iM_{-1} [k^{-1} \partial_z (\hat{\tau}_{Vz} + i\hat{\tau}_{Hz}) + k(\hat{\tau}_{zz} - 2\hat{T})](k, m-1) \\ &+ iM_{+1} [k^{-1} \partial_z (\hat{\tau}_{Vz} - i\hat{\tau}_{Hz}) + k(\hat{\tau}_{zz} - 2\hat{T})](k, m+1) + M_z \hat{\tau}_{Hz}(k, m), \end{aligned} \quad (65)$$

$$\frac{2}{3\beta} \hat{m}_z(k, m) = M_{-1} k^{-1} (\hat{\tau}_{Vz} + i\hat{\tau}_{Hz})(k, m-1) - M_{+1} k^{-1} (\hat{\tau}_{Vz} - i\hat{\tau}_{Hz})(k, m+1) + M_z (\hat{\tau}_{zz} - \hat{T})(k, m). \quad (66)$$

Because \hat{u}_i and $\hat{\tau}_{iz}$ ($i = z, V, H$) are expressed in the form of eq. (50), the magnetization is also expressed in the form of eq. (55). Note that the z -derivative of $\hat{\tau}_{iz}$ is also expressed as a linear combination of $\hat{\tau}_{jz}$ and \hat{u}_j ($i, j = z, V, H$) because of eqs (42)–(47).

3.5 Correction of the contribution from a singular point

The derivation of the piezomagnetic field so far is incorrect for the case where the source is in a layer with non-zero magnetization because the stress tensor expressed by eqs (5)–(10) is incorrect at the source point. The contribution to the magnetic field from the vicinity of the source point must be considered and be added as a correction term.

To find the correction term, the following three virtual distributions of magnetization labelled by Type-0, Type-1 and Type-2 should be considered, as illustrated in Fig. 2, and the corresponding magnetization $H^{\text{TYPE-}n}$ ($n = 1, 2, 3$) denoted. In the Type-0 distribution, magnetization is described by eq. (11) combined with eqs (5)–(10) in the entire space and is thus incorrect at the source point. Type-1 and Type-2 are defined by replacing magnetizations in a portion of the Type-0 distribution by zero. In the Type-1 and Type-2 distributions, magnetizations in a layer $z_s - \epsilon/2 < z < z + \epsilon/2$ and in a sphere centred at the source $(0, 0, z_s)$ with a radius of $\epsilon/2$ are set to zero, respectively.

The correct magnetic field H^{correct} is obtained by taking $\epsilon \rightarrow +0$ in the Type-2 solution:

$$H^{\text{correct}} \equiv \lim_{\epsilon \rightarrow +0} H^{\text{Type-2}(\epsilon)}, \quad (67)$$

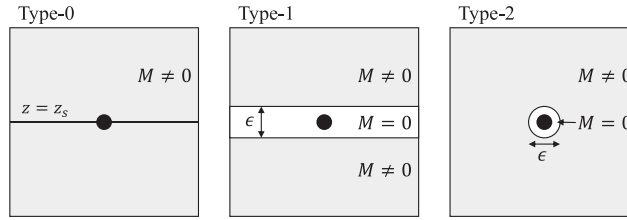


Figure 2. Schematic showing Type-0, Type-1 and Type-2 distributions of magnetization. In each panel, the solid circle represents the source point, and grey and white regions represent magnetized and non-magnetized regions, respectively.

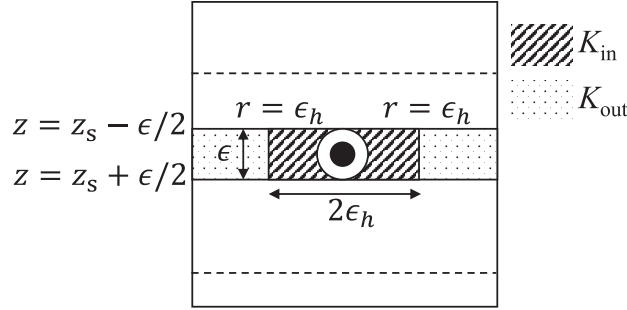


Figure 3. Schematic explaining the validity of using the correction terms derived by Sasai (1991a). The solid circle represents a singular point. Shaded and dotted regions represent K_{in} and K_{out} regions, respectively (see the main text in Section 3.4). The parameter ϵ is as defined in Fig. 2, and ϵ_h represents the radius of the cylinder region K_{in} .

where $H^{\text{Type}-n(\epsilon)}$ represents $H^{\text{Type}-n}$ for a specific value of ϵ . Because the solution derived in the previous subsections is $H^{\text{Type}-0}$, the correction term

$$\Delta H = \left[\lim_{\epsilon \rightarrow +0} H^{\text{Type}-2(\epsilon)} \right] - H^{\text{Type}-0} \quad (68)$$

needs to be added to calculate the correct value by $H^{\text{correct}} = H^{\text{Type}-0} + \Delta H$. Considering that the magnetic field (H) is continuous at each boundary and that the governing equations of the magnetic field in the wavenumber domain do not involve singular points, $H^{\text{Type}-0}$ and $H^{\text{Type}-1(\epsilon)}$ are related as $H^{\text{Type}-0} = \lim_{\epsilon \rightarrow +0} H^{\text{Type}-1(\epsilon)}$. Therefore, the correction term is given by

$$\Delta H = \lim_{\epsilon \rightarrow +0} [H^{\text{Type}-2(\epsilon)} - H^{\text{Type}-1(\epsilon)}]. \quad (69)$$

The difference between $H^{\text{Type}-1(\epsilon)}$ and $H^{\text{Type}-2(\epsilon)}$ has been investigated in detail by Sasai (1991a), who considered this problem in a medium with uniform elasticity, which differs from the approach of the present study. However, the same result can be used for a medium with a layered structure of elasticity, as justified by the following consideration. For the Type-1 distribution, let the region $z_s - \epsilon/2 < z < z_s + \epsilon/2$ be divided into two parts, K_{in} and K_{out} , which are inside and outside the cylinder centred at the source with radius $\epsilon_h/2$ (Fig. 3). The value ϵ_h must be larger than ϵ ; nevertheless, ϵ_h can take an arbitrary small value because only the limitation of $\epsilon \rightarrow +0$ is considered. When ϵ approaches zero while ϵ_h is fixed to an arbitrary value, the contribution to the magnetic field from the K_{out} region converges to zero because no singular point of the magnetization exists in K_{out} . This means that the difference between magnetic fields corresponding to Type-1(ϵ) and Type-2(ϵ) distribution arises only from the K_{in} region. When ϵ_h is sufficiently small relative to the distance between the source level and the nearest elastic boundary, the stress distribution in the K_{in} region is almost the same as that calculated for a medium with uniform elasticity and converges to the identical distribution when $\epsilon_h \rightarrow +0$. Therefore, using the correction term ΔH given by Sasai (1991a) for the present layered elasticity model is justified. Explicit forms of ΔH are given in Appendix C.

3.6 Changes in the total force of the geomagnetic field

In practice, changes in the total geomagnetic force, denoted by ΔF , are frequently observed instead of each component of the magnetic field because ΔF is most precisely determined. The geomagnetic total force F is given by $F = |\mathbf{B}^g + \Delta \mathbf{B}|$, where \mathbf{B}^g is the surrounding geomagnetic field and $\Delta \mathbf{B} = (\Delta B_x, \Delta B_y, \Delta B_z)$ is the change in magnetic induction due to the piezomagnetic effect. Note that ΔB_i ($i = x, y, z$) has been denoted by B_i to simplify the notation so far in this paper. Because $|\Delta \mathbf{B}| \ll |\mathbf{B}^g|$, the change in F (i.e. ΔF) is evaluated by

$$\Delta F = l_x \Delta B_x + l_y \Delta B_y + l_z \Delta B_z, \quad (70)$$

where (l_x, l_y, l_z) is the cosine of the direction of the surrounding geomagnetic field. However, ΔF defined by this expression is inappropriate for comparison with the observed value of ΔF when the observation is performed below ground level. When ΔF is measured below ground

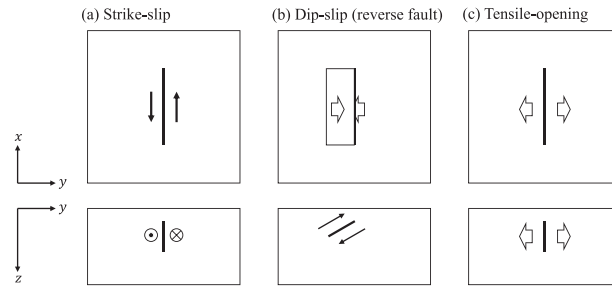


Figure 4. Schematic of (a) strike-slip, (b) dip-slip and (c) tensile-opening models. Upper and lower panels show x - y plan views and vertical y - z cross-sections, respectively.

Table 1. Default parameters adopted for calculating the piezomagnetic field.

Fault length	10 km
Fault width	5 km
Depth of burial	0.5 km
Dislocation ^a	1 m
Rigidity of upper layer ($G_1 = \lambda_1$)	30 GPa
Initial magnetization	1 A m ⁻¹
Stress sensitivity	1×10^{-9} Pa ⁻¹
Curie depth ^a	15 km
Magnetic inclination	45°
Magnetic declination	0°

^aThese values are changed in case studies.

level, the measurement can be performed only in a hole for installing an instrument, for which the pre-existing volume with magnetization must be removed; therefore, ΔH_i and ΔB_i ($i = x, y, z$) calculated by the layered model are not the same as the actual values. Near the ground surface, a revised formula of eq. (70) to convert the calculated ΔH_i and ΔB_i to an observable ΔF is

$$\Delta F = \mu_0 (I_x \Delta H_x + I_y \Delta H_y) + I_z \Delta B_z, \quad (71)$$

which is continuous at ground level.

3.7 Summary of the procedure for determining the piezomagnetic field

Now the point source problem is completely solved, for which the procedure is summarized as follows. For given strain nuclei, the displacement–stress field in the wavenumber domain is given in the form of eq. (50), together with the expressions listed in Appendix A. Using the displacement–stress field, the type-I distribution of the magnetization (Fig. 2) in the form of eq. (55) is determined by using eqs (64)–(66). The corresponding magnetic field in the form of eq. (56) is determined by using the expressions listed in Appendix B. After transforming these results into the real domain by using eqs (39)–(41) and adding the correction term (eq. 69 and Appendix C), the magnetic field in the real domain is obtained. Changes in the total force of the geomagnetic field are calculated by using eq. (71).

4 NUMERICAL EXAMPLES AND DISCUSSION

To explore how the existence of the elastic contrast affects (or does not affect) the generated piezomagnetic field, some examples of the piezomagnetic field arising from finite faults with different mechanisms are considered. Three types of dislocation source are assumed: (a) a vertical left-lateral strike-slip fault, (b) a reverse fault with a dip angle of 30° and (c) a vertical tensile-opening fault, as illustrated in Fig. 4.

For the calculation, the finite rectangular fault is divided into smaller segments: 100 segments in the strike direction and five segments in the dip direction. The dislocation on each segment is approximated by a point dislocation at its centroid. The size of the segments in the strike direction is 100 m. The sizes of segments in the dip direction are 500, 500, 1000, 1000 and 1000 m. The sizes of shallower segments are set smaller than those of deeper segments because the piezomagnetic field from shallower segments is larger than those from deeper segments. The piezomagnetic and displacement fields generated by dislocation on a finite fault are determined by summing the contributions from all segments. It can be confirmed that the calculated piezomagnetic and displacement fields through this approximation are sufficiently accurate for the following discussion, as graphically explained in Appendix D.

In the following calculations, parameters listed in Table 1 are adopted unless otherwise mentioned. Concerning the piezomagnetic field, only ΔF calculated by eq. (71) is considered. The piezomagnetic and displacement fields are evaluated at a depth of $z = 1$ m. The direction

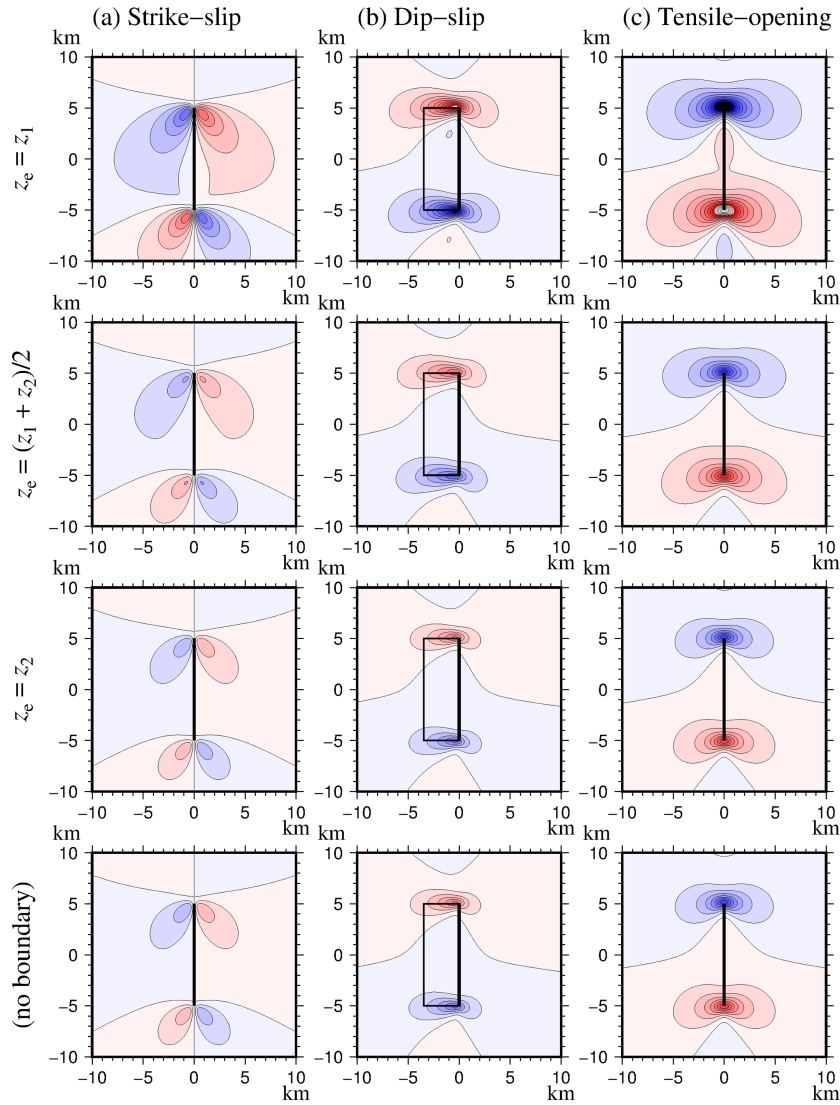


Figure 5. Dependence of the piezomagnetic field on the depth of the elastic boundary, assuming uniform slip. A rectangular fault with (a) strike-slip, (b) dip-slip and (c) tensile-open is assumed as the dislocation source. The top, second and third rows show results for which the depth of the elastic contrast z_e is set to z_1 , $(z_1 + z_2)/2$ and z_2 , respectively, whereas the bottom row shows results for no elastic boundary. Values z_1 and z_2 represent the depths of the top and bottom of the fault, respectively. Red and blue colours show positive and negative signals, respectively, and contour intervals are 0.5 nT.

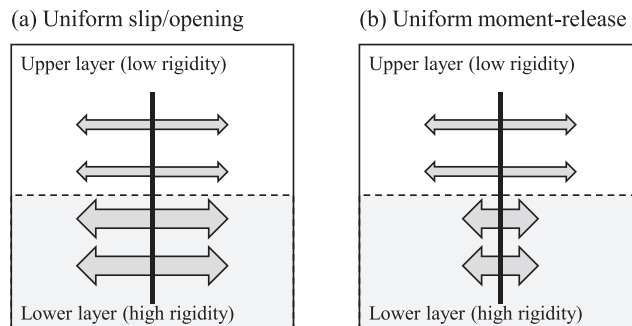


Figure 6. Schematic to explain ‘uniform slip’ (a) and ‘uniform moment-release’ (b) settings for the tensile-opening case. A two-layered model is exemplified in which the rigidity of the lower layer is higher than that of the upper. Thick and dashed lines represent the fault plane and the rigidity boundary, respectively. The length and width of arrows represent the size of opening and *in situ* rigidity, respectively, and therefore their product (i.e. the area of each arrow symbol) represents moment-release.

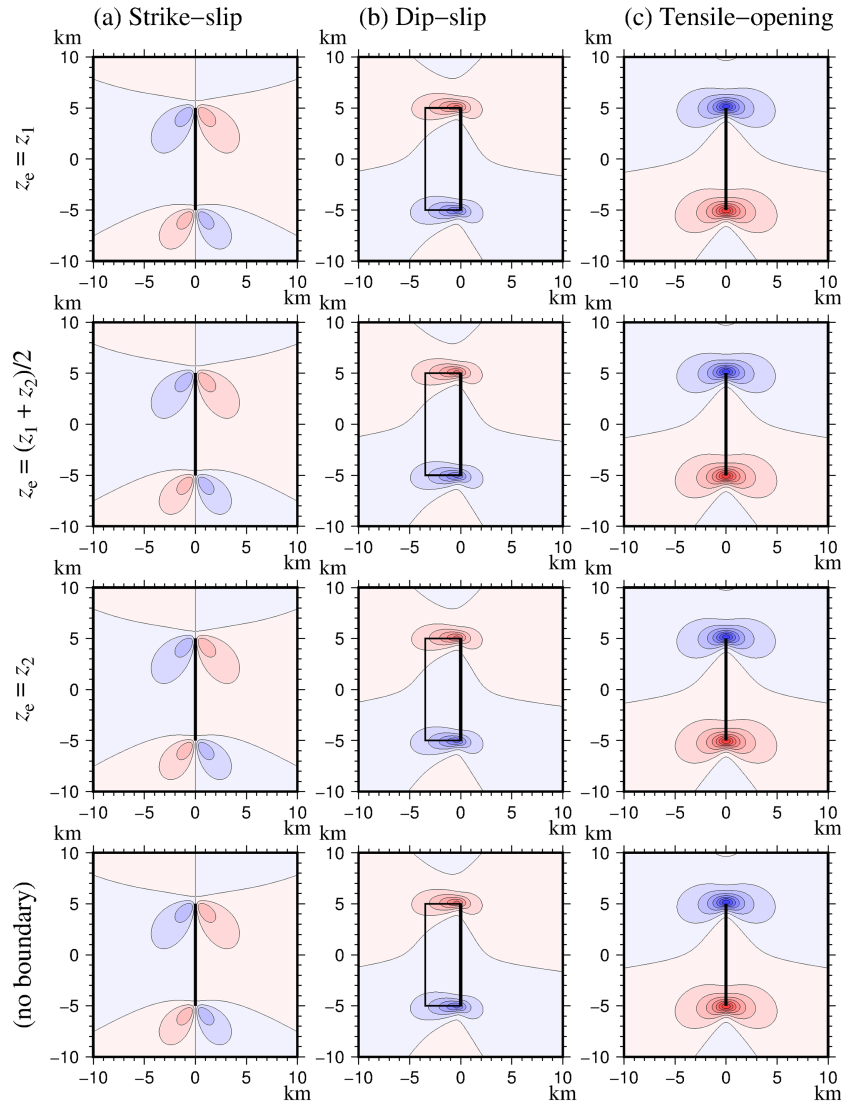


Figure 7. As in Fig. 5, but with the moment-release, not the slip or opening, fixed to the same value in all cases.

of the initial magnetization is set to be the same as that of the ambient geomagnetic field. The intensity of the initial magnetization ($|M|$) and the stress sensitivity (β) are set to constant values above the Curie point depth, although different intensities can be assigned to different layers in the present scheme.

4.1 Dependence of the piezomagnetic field on the boundary depth

First, the piezomagnetic fields for the three models presented in Fig. 4 are calculated with dislocation (i.e. slip or opening) over the rectangular source area being set to be uniform, as always assumed in previous theoretical works (e.g. section 3 of Utsugi *et al.* 2000). Fig. 5 shows the results for cases with elastic boundaries set at the top, middle, and bottom of the fault, and with no elastic boundary.

As can be clearly observed, the expected piezomagnetic fields for shallow boundary cases are larger than those for deep boundary cases in all three mechanisms, whereas their spatial patterns are highly similar for all mechanisms. This result appears to indicate that a shallow elastic boundary enhances the piezomagnetic field whereas a deep boundary does not.

The above setting of parameters may be inappropriate for discussing the role of variations in rigidity. To calculate the results presented in Fig. 5, it was assumed that the slip/opening is uniform over a rectangular fault. However, the moment-release on the fault under this assumption is not uniform when the fault crosses the elastic boundary. The moment-release from each segment of a fault is proportional to the rigidity at the point of the segment. It may be appropriate to compare results between ‘uniform moment-release’ settings rather than ‘uniform slip/opening’ settings as adopted in Fig. 5 (Fig. 6). Note that the ‘uniform slip/opening’ and ‘uniform moment-release’ settings correspond to the centre of dilatation (COD) and centre of pressure (COP) models, respectively, in the case of spherical sources; piezomagnetic fields from COD and COP models are compared in Currenti *et al.* (2011). Note also that the source fault is divided into segments in such a way

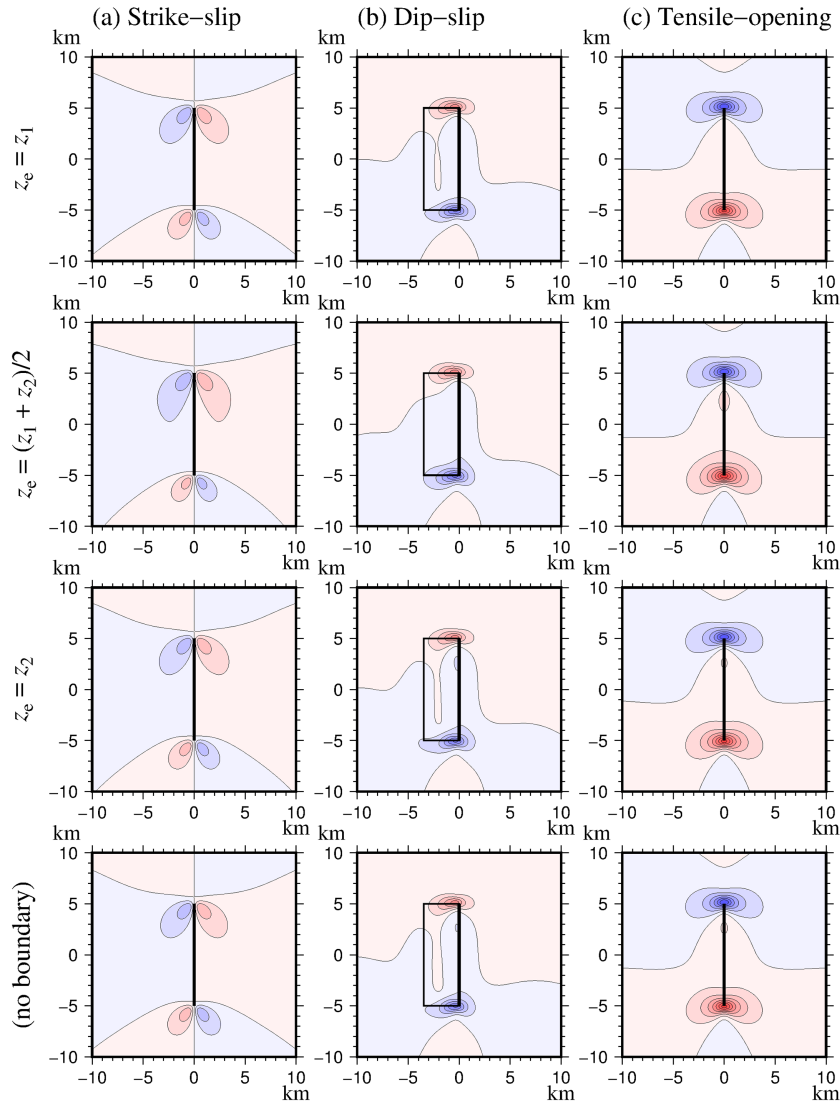


Figure 8. As in Fig. 5, but with the Curie point depth set to the middle depths of the rectangular sources, which are 2.5 km for the strike-slip and tensile-opening models and 1.5 km for the dip-slip model. Note that the depth of the elastic boundary is the same as the Curie point depth in the cases of the second row.

that each segment is in the same layer. The piezomagnetic fields arising from such a segment with the ‘uniform slip/opening’ and ‘uniform moment-release’ settings can be calculated by rescaling: the piezomagnetic field arising from the latter is calculated by multiplying that from the former by a factor determined by the assumed rigidity, and vice versa by dividing.

Fig. 7 shows the resulting piezomagnetic fields with the uniform moment-release setting, with other parameters and configurations being the same as those adopted in the previous example (Fig. 6). Note that when the entire fault area is shallower than the elastic boundary, the dislocation of this case is the same as that of the previous example.

In contrast to the previous example (Fig. 5), no differences are observed in the present example (Fig. 7). This shows that the existence of the elastic boundary does not alter the resulting piezomagnetic field when the moment-release is uniform over a fault.

The examples presented so far assumed that the depth of the Curie point isotherm is 15 km, which is far below the depth of the assumed elastic boundaries. To obtain a firm conclusion, the piezomagnetic field arising from a model for a situation in which the Curie point isotherm is shallower should also be examined. For the case where the Curie point depth is close to the depth of the elastic boundary, the piezomagnetic field arising from models with a shallow Curie point depth located in the middle part of the fault was considered. The depth of the Curie point was set to 2.5 km for strike-slip and tensile-opening models, and 1.5 km for the dip-slip model. The uniform moment-release setting was adopted. Values of other parameters were the same as those adopted in calculations for Figs 5 and 7. Results are shown in Fig. 8.

In contrast to the previous case (Fig. 7), there are some differences in the piezomagnetic field depending on the depth of the elastic boundary. For example, the piezomagnetic field arising from the strike-slip model with $z_e = 2.5$ km (i.e. the second subpanel of Fig. 8a) shows a wide spatial extent near the northern edge compared with those with other z_e values (i.e. the top, third, and bottom subpanels of Fig. 8a). However, the difference is as small as 0.1 nT, which is below the detection limit of observation (~ 1.0 nT). Similar results are obtained for dip-slip and tensile-opening models (Figs 8b and c). In summary, the piezomagnetic field resulting from a crust with a horizontal elastic

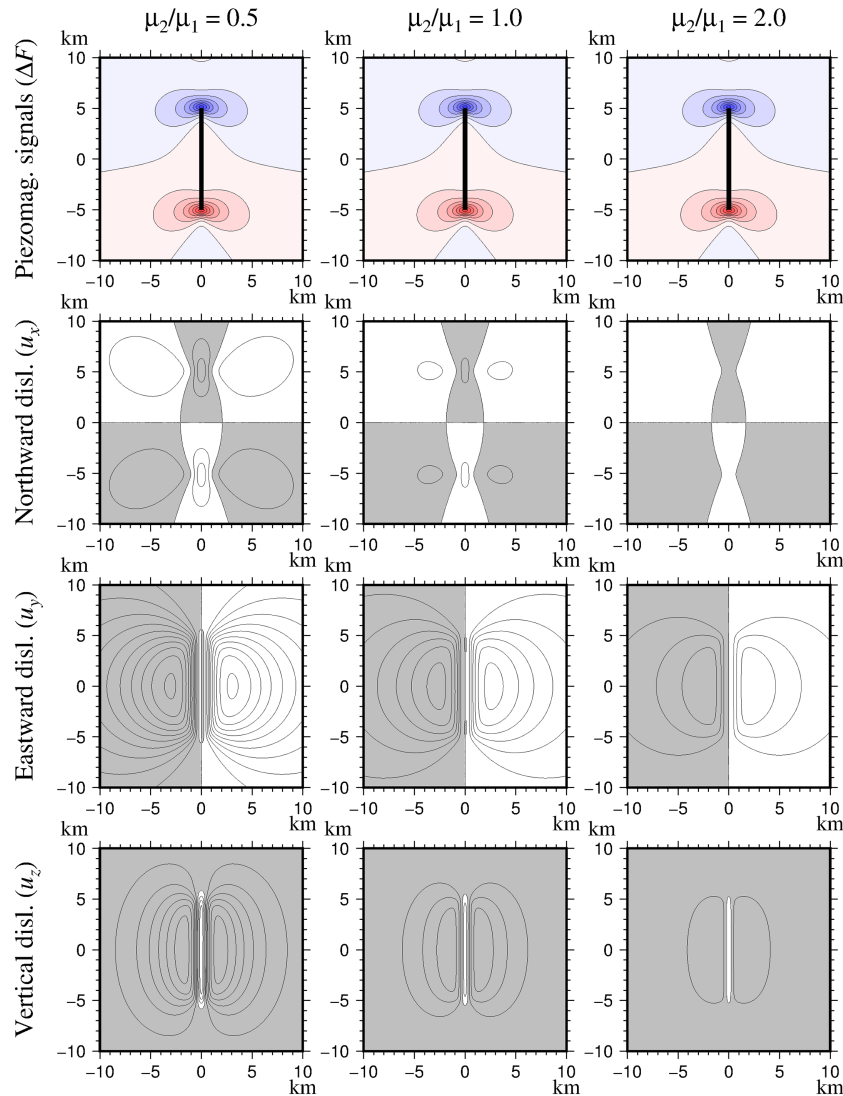


Figure 9. Comparison of the dependence of the piezomagnetic field and surface dislocation on the ratio of the rigidity of the lower layer to that of the upper layer (μ_2/μ_1). A tensile-opening fault (as illustrated in Fig. 4c) is assumed as the dislocation source. The magnitudes of dislocation are set to the same value of 1 m in all cases. The depth of the elastic boundary is set to 0.5 km, corresponding to the top of the fault. In the top panels (of ΔF), red and blue represent positive and negative changes, respectively. Contour intervals are 0.5 nT. The black line in each panel represents the position of the fault. In the panels of u_x , u_y and u_z , white represents northward, eastward and upward dislocation, respectively, and grey the opposite. Contour intervals are 5 cm.

boundary is not significantly different from that resulting from a crust with uniform elasticity, even when the elastic boundary is located near the Curie point depth.

The present result seems to be inconsistent with that of Okubo & Oshiman (2004), who demonstrated that the piezomagnetic field arising from the Mogi model, that is, a point pressure source embedded in a demagnetized sphere, is substantially influenced by the existence of an elastic boundary, particularly when the depth of the elastic boundary is close to that of the pressure source. A possible interpretation of this discrepancy is the difference in magnetization structure between the two models. In the present study, it is assumed that the magnetization is uniform in the horizontal direction. In contrast, the magnetization is assumed to be zero near the pressure source in the Mogi model so as to represent demagnetization around hot magma, meaning that the Mogi model involves marked variation in magnetization in the horizontal direction. Many previous studies assuming uniform rigidity have pointed out that the piezomagnetic field is substantially enhanced by magnetization boundaries (e.g. Oshiman 1990; Yamazaki, 2009, 2011). It is natural to assume that this enhancement mechanism also works in the case of a layered rigidity structure.

If the given interpretation of the discrepancy between the insights derived from the present model and those of the Mogi model is correct, the existence of a rigidity contrast will play an important role only when there are horizontal variations in magnetization. This means that heterogeneities in rigidity do not need to be considered when observing and interpreting the piezomagnetic field over an area in which magnetization is horizontally uniform as long as the moment-release on the fault is precisely given, in which case the calculation of such heterogeneities will provide an accurate estimation of the piezomagnetic field. In this sense, many earlier results for the piezomagnetic field

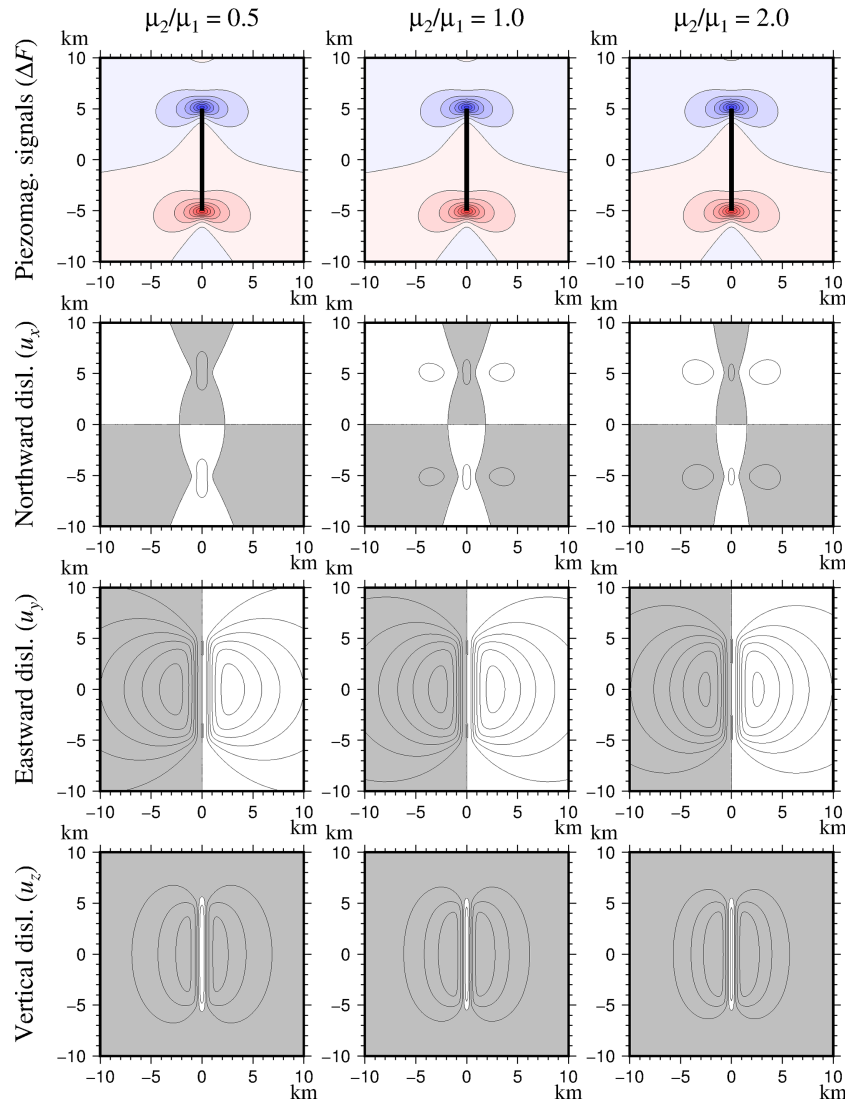


Figure 10. As in Fig. 9, but with the depth of the elastic boundary set to 4.5 km, corresponding to the bottom of the fault.

are considered to be sufficiently accurate. In contrast, heterogeneities in rigidity must be considered when observing and interpreting the piezomagnetic field over an area in which magnetization is horizontally non-uniform, such as is expected in geothermal areas. The calculation procedure developed in the present study cannot be applied to such cases.

4.2 Comparisons between the piezomagnetic and displacement fields

It is interesting to consider the displacement field corresponding to the obtained piezomagnetic field because the displacement field provides more fundamental information on subsurface dislocation sources than does the piezomagnetic field. To compare the influences of elastic heterogeneities on the piezomagnetic and displacement fields, both fields were calculated and compared for the same models. As an example, a tensile-opening rectangular fault (Fig. 4c) is assumed. In the calculation, the Curie point depth and the rigidity of the upper layer are fixed to the values in Table 1, and the ratio of rigidity, namely, μ_2/μ_1 , is assumed to be 0.5, 1.0 or 2.0. The depth of the rigidity boundary is assumed to coincide with the top (0.5 km) or the bottom (4.5 km) of the fault.

The uniform opening setting (Fig. 6a) is considered first. Figs 9 and 10 present the results for models with shallow (0.5 km) and deep (4.5 km) elastic boundaries, respectively. In the case of the shallow boundary (Fig. 9), a contrast is clearly recognized between the dependence of the piezomagnetic and dislocation fields on the ratio of rigidity: the piezomagnetic field is approximately proportional to μ_2/μ_1 , whereas the amplitude of the displacement field is less sensitive to the ratio μ_2/μ_1 . In contrast, in the case of the deep boundary (Fig. 9), both the piezomagnetic and dislocations are essentially independent of the ratio μ_2/μ_1 .

The uniform moment-release setting (Fig. 6b) is also considered, as in Fig. 7. The depth of the rigidity boundary is assumed to coincide with the top of the fault (0.5 km). Fig. 11 presents the results. Note that the piezomagnetic and displacement fields resulting from this setting are obtained simply by multiplying the reciprocal of μ_2/μ_1 by the results for the uniform opening setting (Fig. 9). In contrast to the results

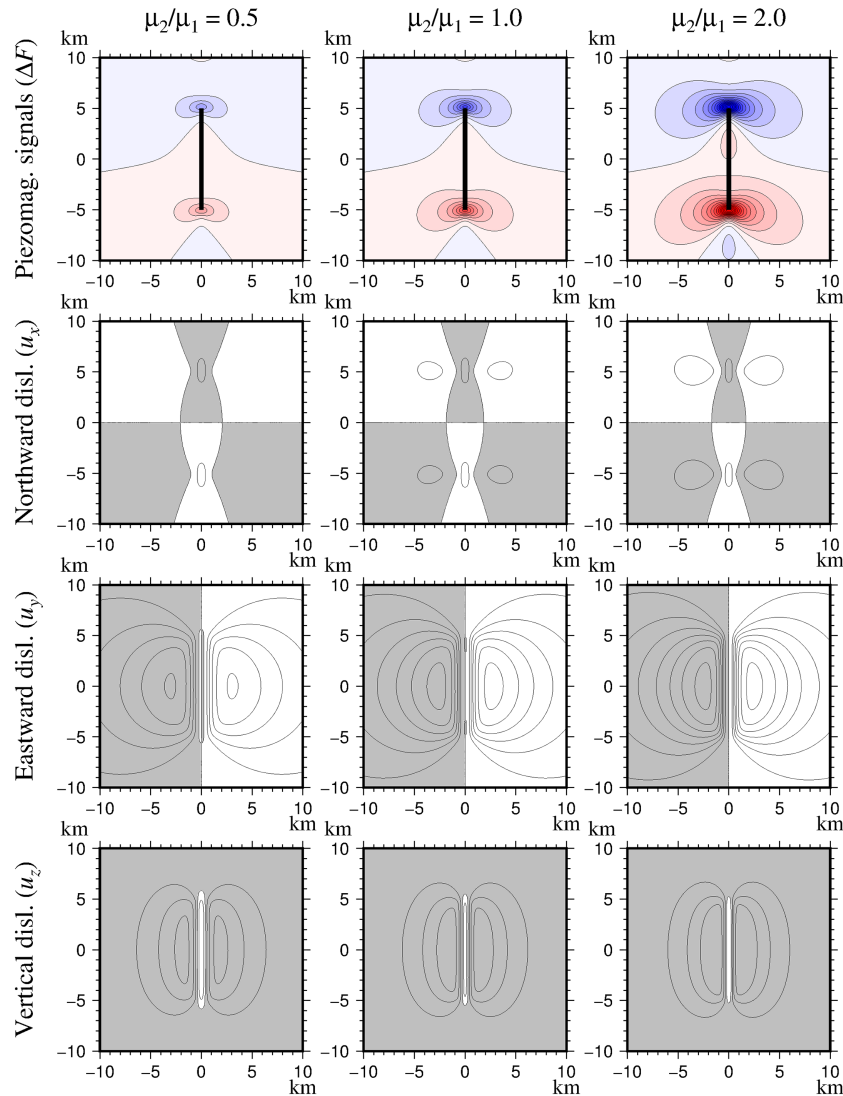


Figure 11. As in Fig. 9, but with the magnitudes of moment, not dislocation, set to the same value.

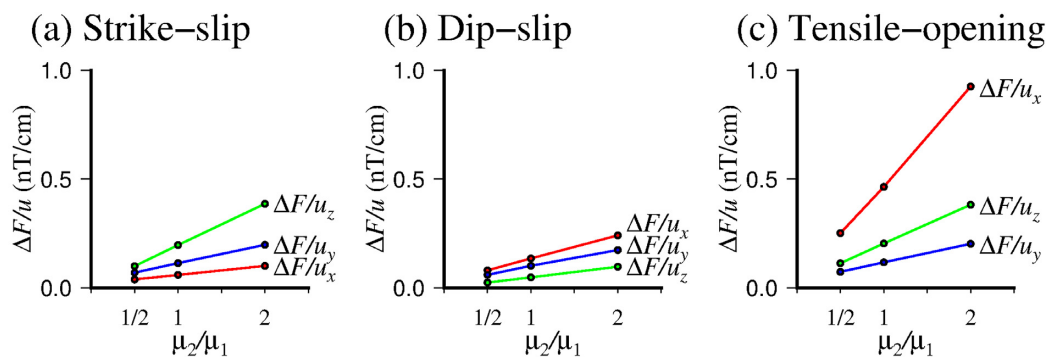


Figure 12. Ratios between the maximum amplitudes of the piezomagnetic (ΔF) and displacement (u_x , u_y and u_z) fields generated by a dislocation on a rectangular fault with three mechanisms, and their dependence on the ratio of the rigidity of the lower layer (μ_2) to that of the upper layer (μ_1), respectively.

for the uniform opening setting (Fig. 9), the piezomagnetic field for the uniform moment-release setting is almost independent of the ratio μ_2/μ_1 except for minor differences, whereas the displacement field depends strongly on the ratio μ_2/μ_1 .

The ratio between the maximum amplitude of the piezomagnetic field and the dislocation becomes larger/smaller than that expected for a uniform rigidity model when the rigidity near the dislocation source is larger/smaller than that of the shallower part. Similar results to the tensile-opening model are obtained for the other source mechanisms, namely, strike- and dip-slip faulting and for other components, as summarized in Fig. 12.

In many studies of the piezomagnetic field (e.g. Utada *et al.* 2011; Yamazaki 2013), the size of slip/opening on the fault estimated by means of geodetic inversion is assumed to estimate the corresponding piezomagnetic field. The above results imply that the size of slip or opening estimated by geodetic data with the assumption of uniform rigidity is fairly accurate even when the rigidity is non-uniform but the piezomagnetic field is not. The piezomagnetic field becomes smaller/larger than the actual field depending on whether the rigidity of the deep crust is smaller/larger than the rigidity of the shallow crust. In Earth's crust, an increase in rigidity with increasing depth is quite common. Therefore, it is possible that many previous results for the piezomagnetic field are likely to be underestimations.

The possible misestimation of the piezomagnetic field might have influenced some earlier interpretations of the piezomagnetic effect in geophysics. In particular, it may have affected estimations of the stress sensitivity β (e.g. Nishida *et al.* 2007; Utada *et al.* 2011; Yamazaki 2013), which is based on the calculated amplitude of piezomagnetic signals. However, the dependency of the piezomagnetic field on the elastic structure also implies the potential usefulness of observing the piezomagnetic field. The simultaneous use of the piezomagnetic and displacement fields might provide quantitative information on the difference between rigidities near the surface and near the dislocation source, which is difficult to estimate using solely geodetic means.

5 CONCLUSIONS

A semi-analytical formula for calculating the piezomagnetic field arising from a point dislocation source embedded in a layered elastic medium is derived. All of the governing equations, written as partial differential equations in a real domain together with the linear constitutive law of the piezomagnetic effect, are converted to a set of ordinary differential equations in a wavenumber domain. Equations in the wavenumber domain can be solved analytically, and each component of the piezomagnetic field in the real domain is obtained after applying the Hankel transform.

When the moment-release at the dislocation source is fixed, the effect of rigidity differences between the upper and lower layers on the piezomagnetic field is minor even in the case where the Curie point depth is near the source of dislocation. This result differs from that of a previous study that assumed the Mogi model, suggesting that heterogeneities of magnetization in the horizontal direction may be of importance when combined with layered rigidity structures.

A contrast is observed between the piezomagnetic and displacement fields corresponding to models with layered rigidity structures. The piezomagnetic field is roughly proportional to the moment-release on a source fault, whereas the displacement field is proportional to the slip/opening on the fault. In cases where the rigidity of the crust increases with increasing depth, the results of calculation of the piezomagnetic field may have been underestimated in many previous studies that assumed uniform rigidity and a geodetically inverted amount of slip.

ACKNOWLEDGEMENTS

FORTTRAN subroutines coded by Takuya Ooura (Research Institute for Mathematical Sciences, Kyoto University, Japan; url: <http://www.kurims.kyoto-u.ac.jp/~ooura/index.html>; last accessed on 29 October 2019) were used after some modification, in which the double-exponential formula for numerical integration (Ooura & Mori 1991) was used to perform the Hankel transform. The Generic Mapping Tools (GMT) package version 5 (Wessel *et al.* 2013) was used to draw some figures and to interpolate discrete numerical results into evenly spaced grid points. Takuto Minami (Kobe University, Japan) pointed out some typographical errors in mathematical formulation in an earlier version of the manuscript. Comments by Gilda Currenti and an anonymous reviewer helped to improve an earlier version of the manuscript. Advice from associate editor Eduard Petrovsky is also acknowledged. Stallard Scientific Editing helped to improve the language of the paper. This work was partially supported by JSPS KAKENHI Grant Number JP17K05634.

Data Availability

The computation code written in FORTRAN 90 and using GMT 5.4.1 will be shared with the corresponding author upon request, except for a subroutine that was provided by a third party and then modified and whose redistribution of its modified version is not permitted. Intermittent and final numbers used to draw figures in this paper will also be shared upon request.

REFERENCES

- Aki, K. & Richards, P.G., 2002. *Quantitative Seismology*, 2nd edn, University Science Books, 704pp.
- Currenti, G., Del Negro, C., Di Stefano, A. & Napoli, R., 2009. Numerical simulation of stress induced piezomagnetic fields at Etna volcano, *Geophys. J. Int.*, **179**, 1469–1476.
- Currenti, G., Del Negro, C., Johnston, M. & Sasai, Y., 2007. Close temporal correspondence between geomagnetic anomalies and earthquakes during the 2002–2003 eruption of Etna volcano, *J. geophys. Res.*, **112**, B09103, doi:10.1029/2007JB005029.
- Currenti, G., Del Negro, C., & Sasai, Y., 2008. Time dependent piezomagnetic fields in viscoelastic medium. *Geophys. J. Int.*, **172**, 536–548.
- Currenti, G., Napoli, R., Di Stefano, A., Greco, F. & Del Negro, C., 2011. 3D integrated geophysical modeling for the 2008 magma intrusion at Etna: constraints on rheology and dike overpressure, *Phys. Earth planet. Inter.*, **185**, 44–52.
- Del Negro, C. & Currenti, G., 2003. Volcanomagnetic signals associated with the 2001 flank eruption of Mt. Etna (Italy), *Geophys. Res. Lett.*, **30**(7), doi:10.1029/2002GL015481

- Del Negro, C., Currenti, G., Napoli, R. & Vicari, A., 2004. Volcanomagnetic changes accompanying the onset of the 2002–2003 Eruption of Mt. Etna (Italy), *Earth planet. Sci. Lett.*, **229**, 1–14.
- Fukahata, Y. & Matsu'ura, M., 2005. General expressions for internal deformation fields due to a dislocation source in a multilayered elastic half-space, *Geophys. J. Int.*, **161**, 507–521.
- Johnston, M.J.S., 1997. Review of electric and magnetic fields accompanying seismic and volcanic activity, *Surv. Geophys.*, **18**, 441–476.
- Johnston, M.J.S. & Mueller, R.J., 1987. Seismomagnetic observation with the July 8, 1986 Magnitude 5.9 North Palm Springs earthquake, *Science*, **237**, 1201–1203.
- Johnston, M.J.S., Mueller, R.J. & Sasai, Y., 1994. Magnetic field observations in the near-field of the 28 June 1992 M_w 7.3 Landers, California, earthquake, *Bull. seism. Soc. Am.*, **84**, 792–798.
- Johnston, M.J.S., Sasai, Y., Egbert, G.D. & Mueller, R.J., 2006. Seismomagnetic effects from the long-awaited 28 September 2004 $M_6.0$ Parkfield earthquake, *Bull. seism. Soc. Am.*, **96**(4B), S206–S220.
- Kennett, B.L.N., 2009. *Seismic Wave Propagation in Stratified Media*, new edn, ANU E Press, 288pp.
- Kennett, B.L.N. & Kerry, N.J., 1979. Seismic waves in a stratified halfspace, *Geophys. J. R. Astr. Soc.*, **57**, 557–583.
- Nagata, T., 1970. Basic magnetic properties of rocks under the effects of mechanical stress, *Tectonophysics*, **9**, 167–195.
- Napoli, R., Currenti, G., Del Negro, C., Greco, F. & Scandura, D., 2008. Volcanomagnetic evidence of the magmatic intrusion on 13th May 2008 Etna eruption, *Geophys. Res. Lett.*, **35**, L22301, doi:10.1029/2008GL035350
- Nishida, Y., Utsugi, M. & Mogi, T., 2007. Tectonomagnetic study in the eastern part of Hokkaido, NE Japan (II): Magnetic fields related with the 2003 Tokachi-oki earthquake and the 2004 Kushiro-oki earthquake, *Earth Planets Space*, **59**, 1181–1186.
- Ohnaka, M. & Kinoshita, H., 1968. Effects of uniaxial compression on remanent magnetization, *J. Geomagn. Geoelectr.*, **20**, 93–99.
- Okada, Y., 1992. Internal deformation due to shear and tensile faults in a half-space, *Bull. seism. Soc. Am.*, **82**, 1018–1040.
- Okubo, A. & Kanda, W., 2010. Numerical simulation of piezomagnetic changes associated with hydrothermal pressurization, *Geophys. J. Int.*, **181**, 1343–1361.
- Okubo, A. & Oshiman, N., 2004. Piezomagnetic field associated with a numerical solution of the Mogi model in a non-uniform elastic medium, *Geophys. J. Int.*, **159**, 509–520.
- Ooura, T. & Mori, M., 1991. The double exponential formula for oscillatory functions over the half infinite interval, *J. Comput. Appl. Math.*, **38**, 353–360.
- Oshiman, N., 1990. Enhancement of tectonomagnetic change due to non-uniform magnetization in the Earth's crust – two-dimensional case studies, *J. Geomagn. Geoelectr.*, **42**, 607–619.
- Oshiman, N., Tuncer, M.K., Honkura, Y., Baris, S., Yazici, O. & Isikara, A.M., 1991. A strategy of tectonomagnetic observation for monitoring possible precursors to earthquakes in the western part of the North Anatolian fault zone, Turkey, *Tectonophysics*, **193**, 359–368.
- Pan, E., 1989. Static response of a transversely isotropic and layered half space to general dislocation sources, *Phys. Earth planet. Inter.*, **58**, 103–117.
- Pozzi, J.P., 1977. Effects of stresses on magnetic properties of volcanic rocks, *Phys. Earth planet. Inter.*, **14**, 77–85.
- Sasai, Y., 1994. Piezomagnetic fields produced by dislocation sources, *Surv. Geophys.*, **15**, 363–382.
- Sasai, Y. & Ishikawa, Y., 1980. Tectonomagnetic event preceding an $M = 5.0$ Earthquake in the Izu Peninsula—aseismic slip of a buried fault?, *Bull. Earthq. Res. Inst. Univ Tokyo*, **55**, 895–911.
- Sasai, Y., 1983. A surface integral representation of the tectonomagnetic field based on the linear piezomagnetic effect, *Bull. Earthq. Res. Inst. Univ Tokyo*, **58**, 763–785.
- Sasai, Y., 1986. A Green's function for tectonomagnetic problems in an elastic half-space, *J. Geomagn. Geoelectr.*, **38**, 949–969.
- Sasai, Y., 1991a. Tectonomagnetic modeling on the basis of the linear piezomagnetic effect, *Bull. Earthq. Res. Inst. Univ Tokyo*, **66**, 585–722.
- Sasai, Y., 1991b. Piezomagnetic field associated with the Mogi model revisited: analytic solution for finite spherical source, *J. Geomagn. Geoelectr.*, **43**, 21–64.
- Sasai, Y. & Ishikawa, Y., 1991. Tectonomagnetic signals related to the seismo-volcanic activity in the Izu Peninsula, *J. Phys. Earth*, **39**, 299–319.
- Sasai, Y., Uyeshima, M., Zlotnicki, J., Utada, H., Kagiya, T., Hashimoto, T. & Takahashi, Y., 2002. Magnetic and electric field observations during the 2000 activity of Miyake-jima volcano, Central Japan, *Earth planet. Sci. Lett.*, **203**, 769–777.
- Shamsi, S & Stacey, F.D., 1969. Dislocation models and seismomagnetic calculations for California 1906 and Alaska 1964 earthquakes, *Bull. seism. Soc. Am.*, **59**, 1435–1448.
- Stacey, F.D., 1964. The seismomagnetic effect, *Pure Appl. Geophys.*, **58**, 5–22.
- Stuart, W.D., Banks, P.O., Sasai, Y. & Liu, S-W., 1995. Piezomagnetic field for Parkfield fault model, *J. geophys. Res.*, **100**, 24101–24 110.
- Takeuchi, H. & Saito, M., 1972. Seismic surface waves, in *Seismology: Surface Waves and Earth Oscillations, Methods in Computational Physics*, Vol. 11, pp. 217–295, Academic Press.
- Ueda, H., Matsumoto, T., Fujita, E., Ukawa, M., Yamamoto, E., Sasai, Y., Irwan, M. & Kimata, F., 2006. Geomagnetic changes associated with the dike intrusion during the 2000 Miyakejima eruptive activity, Japan, *Earth planet. Sci. Lett.*, **245**, 416–426.
- Utada, H., Shimizu, H., Ogawa, T., Maeda, T., Furumura, T., Yamamoto, T., Yamazaki, N., Yoshitake, Y. & Nagamachi, S., 2011. Geomagnetic field changes in response to the 2011 off the Pacific Coast of Tohoku Earthquake and Tsunami, *Earth and Planetary Science Letters*, **311**, 11–27.
- Utsugi, M., Nishida, Y. & Sasai, Y., 2000. Piezomagnetic potentials due to an inclined rectangular fault in a semi-infinite medium, *Geophys. J. Int.*, **140**, 479–492.
- Uyeshima, M., 2007. EM Monitoring of Crustal Processes Including the Use of the Network-MT Observations, *Surv. Geophys.*, **28**, 199–237.
- Wessel, P., Smith, W.H.F., Scharroo, R., Luis, J.F. & Wobbe, F., 2013. Generic Mapping Tools: improved version released, *EOS, Trans. Am. geophys. Un.*, **94**, 409–410.
- Yamazaki, K., 2009. Calculation of the piezomagnetic field arising from uniform regional stress in inhomogeneously magnetized crust. *Earth Planets Space*, **61**, 1163–1168.
- Yamazaki, K., 2011. Enhancement of co-seismic piezomagnetic signals near the edges of magnetization anomalies in the Earth's crust, *Earth Planets Space*, **63**, 111–118.
- Yamazaki, K., 2013. Improved models of the piezomagnetic field for the 2011 M_w 9.0 Tohoku-oki earthquake, *Earth planet. Sci. Lett.*, **363**, 9–15.
- Zlotnicki, J. & Cornet, F.H., 1986. A numerical model of earthquake-induced piezomagnetic anomalies, *J. geophys. Res.*, **91**, 709–718.
- Zlotnicki, J., Pozzi, J.P. & Cornet, F.H., 1981. Investigation of induced magnetization variations caused by triaxial stresses, *J. geophys. Res.*, **86**(B12), 11899–11 909.

APPENDIX A: EXPRESSION OF THE DISPLACEMENT-STRESS FIELD IN THE WAVENUMBER DOMAIN

Below, an example of the expression of the solution for the displacement and stress fields is given in the form of eq. (50). The notation of variables or parameters with superscript ‘PSV’ indicates that they are used only for \hat{u}_z^n , \hat{u}_V^n , $\hat{\tau}_{zz}^n$, and $\hat{\tau}_{Vz}^n$ (i.e. ‘P-SV mode’ in seismology), and the notation with ‘SH’ indicates that they are used only for \hat{u}_H^n and $\hat{\tau}_{Hz}^n$ (i.e. SH mode).

A.1 \hat{u}_H^n and $\hat{\tau}_{Hz}^n$

The governing equations of \hat{u}_H and $\hat{\tau}_{Hz}$ (eqs 46 and 47) in the n th layer (i.e. $z_{n-1} < z < z_n$ for $n \leq N$ and $z_N < z$ for $n = N + 1$), denoted by \hat{u}_H^n and $\hat{\tau}_{Hz}^n$, respectively, are rewritten in the form of

$$\frac{\partial}{\partial z} \begin{pmatrix} k^{-1} \hat{u}_H^n \\ G_n^{-1} k^{-2} \hat{\tau}_{Hz}^n \end{pmatrix} = k \begin{pmatrix} 0 & 1 \\ 1 & 0 \end{pmatrix} \begin{pmatrix} k^{-1} \hat{u}_H^n \\ G_n^{-1} k^{-2} \hat{\tau}_{Hz}^n \end{pmatrix}. \quad (\text{A1})$$

scaling factors k and G_n are included to adjust the dimensions of components.

The general solution of eq. (A1) is expressed in the form of

$$\begin{pmatrix} k^{-1} \hat{u}_H^n \\ G_n^{-1} k^{-2} \hat{\tau}_{Hz}^n \end{pmatrix} = \begin{pmatrix} \underline{d}^{\text{SH}+} & \underline{d}^{\text{SH}-} \end{pmatrix} \begin{pmatrix} e^{-k(z-z_{n-1})} & 0 \\ 0 & e^{-k(z_n-z)} \end{pmatrix} \begin{pmatrix} a_n^{\text{SH}+} \\ a_n^{\text{SH}-} \end{pmatrix}, \quad (\text{A2})$$

where

$$\underline{d}^{\text{SH}+} = \begin{pmatrix} 1 \\ -1 \end{pmatrix}, \quad \underline{d}^{\text{SH}-} = \begin{pmatrix} 1 \\ 1 \end{pmatrix}. \quad (\text{A3})$$

coefficients $a_n^{\text{SH}+}$ and $a_n^{\text{SH}-}$ are determined by boundary conditions. In the bottom layer (i.e. $n = N + 1$), $a_{N+1}^{\text{SH}+} = 0$ to assure the convergence condition at $z \rightarrow \infty$. Note that each component of eq. (A2) is written in the same form as eq. (50), with $\hat{u}_{H,\pm 2}^n$ and $\hat{\tau}_{Hz,\pm 2}^n$ being zero.

Coefficients $a_n^{\text{SH}+}$ and $a_n^{\text{SH}-}$ are determined by boundary conditions (eq. 49). The boundary conditions are expressed as

$$\begin{pmatrix} -1 & e^{-kz_1} \end{pmatrix} \begin{pmatrix} a_1^{\text{SH}+} \\ a_1^{\text{SH}-} \end{pmatrix} = 0, \quad (\text{A4})$$

$$\begin{pmatrix} \underline{d}^{\text{SH}+} e^{-kh_n} & \underline{d}^{\text{SH}-} & -\underline{C}_{n+1}^{\text{SH}} \underline{d}^{\text{SH}+} & -\underline{C}_{n+1}^{\text{SH}} \underline{d}^{\text{SH}-} e^{-kh_{n+1}} \end{pmatrix} \begin{pmatrix} a_n^{\text{SH}+} \\ a_n^{\text{SH}-} \\ a_{n+1}^{\text{SH}+} \\ a_{n+1}^{\text{SH}-} \end{pmatrix} = -\delta_{sn} \underline{\mathcal{S}}^{\text{SH}}, \quad (\text{A5})$$

$$\begin{pmatrix} \underline{d}^{\text{SH}+} e^{-kh_N} & \underline{d}^{\text{SH}-} & -\underline{C}_{N+1}^{\text{SH}} \underline{d}^{\text{SH}+} \end{pmatrix} \begin{pmatrix} a_N^{\text{SH}+} \\ a_N^{\text{SH}-} \\ a_{N+1}^{\text{SH}+} \end{pmatrix} = -\delta_{sN} \underline{\mathcal{S}}^{\text{SH}}, \quad (\text{A6})$$

where

$$\underline{C}_{n+1}^{\text{SH}} = \begin{pmatrix} 1 & 0 \\ 0 & G_{n+1} G_n^{-1} \end{pmatrix}, \quad (\text{A7})$$

$$h_n = z_n - z_{n-1}, \quad (\text{A8})$$

and where δ_{sn} is the Kronecker delta, s is the source level (Fig. 1), and $\underline{\mathcal{S}}^{\text{SH}}$ represents the source vector. Eqs (A4)–(A6) form $2N + 1$ linear algebraic equations so that $2N + 1$ unknown parameters, $a_n^{\text{SH}+}$ ($1 \leq n \leq N + 1$) and $a_n^{\text{SH}-}$ ($1 \leq n \leq N$), are determined for a given $\underline{\mathcal{S}}^{\text{SH}}$.

A.2 \hat{u}_z^n , \hat{u}_V^n , $\hat{\tau}_{zz}^n$ and $\hat{\tau}_{Vz}^n$

The governing equations of \hat{u}_z , \hat{u}_V , $\hat{\tau}_{zz}$ and $\hat{\tau}_{Vz}$ (eqs 42–45) in the n th layer (i.e. $z_{n-1} < z < z_n$ for $n \leq N$ and $z_N < z$ for $n = N + 1$), denoted by \hat{u}_z^n , \hat{u}_V^n , $\hat{\tau}_{zz}^n$ and $\hat{\tau}_{Vz}^n$, respectively, are rewritten in the form of

$$\frac{\partial}{\partial z} \begin{pmatrix} \hat{u}_z^n \\ k^{-1} \hat{u}_V^n \\ G_n^{-1} k^{-1} \hat{\tau}_{zz}^n \\ G_n^{-1} k^{-2} \hat{\tau}_{Vz}^n \end{pmatrix} = k \begin{pmatrix} 0 & 1 - 2t_n & 1 - t_n & 0 \\ 1 & 0 & 0 & 1 \\ 0 & 0 & 0 & -1 \\ 0 & 4t_n & -1 + 2t_n & 0 \end{pmatrix} \begin{pmatrix} \hat{u}_z^n \\ k^{-1} \hat{u}_V^n \\ G_n^{-1} k^{-1} \hat{\tau}_{zz}^n \\ G_n^{-1} k^{-2} \hat{\tau}_{Vz}^n \end{pmatrix} \quad (\text{A9})$$

where

$$t_n = \frac{\lambda_n + G_n}{\lambda_n + 2G_n}. \quad (\text{A10})$$

scaling factors k and G_n are included to adjust the dimensions of components.

The general solution of eq. (A9) is expressed in the form of

$$\begin{pmatrix} \hat{u}_z^n(z) \\ k^{-1}\hat{u}_V^n(z) \\ G_n^{-1}k^{-1}\hat{t}_{zz}^n(z) \\ G_n^{-1}k^{-2}\hat{t}_{Vz}^n(z) \end{pmatrix} = \begin{pmatrix} \underline{d}_n^+ & \underline{d}_n^- \\ \underline{0}_2 & \underline{W}_n^-(z) \end{pmatrix} \begin{pmatrix} \underline{W}_n^+(z) & \underline{0}_2 \\ \underline{0}_2 & \underline{W}_n^-(z) \end{pmatrix} \begin{pmatrix} \underline{a}_n^{\text{PSV}+} \\ \underline{a}_n^{\text{PSV}-} \end{pmatrix}, \quad (\text{A11})$$

where

$$\underline{W}_n^+(z) = \begin{pmatrix} e^{-k(z-z_{n-1})} t_n k z e^{-k(z-z_{n-1})} \\ 0 & e^{-k(z-z_{n-1})} \end{pmatrix}, \quad \underline{W}_n^-(z) = \begin{pmatrix} e^{-k(z_n-z)} -t_n k z e^{-k(z_n-z)} \\ 0 & e^{-k(z_n-z)} \end{pmatrix}, \quad (\text{A12})$$

$$\underline{d}_n^+ = \begin{pmatrix} \underline{d}_n^{+1} & \underline{d}_n^{+2} \end{pmatrix}, \quad \underline{d}_n^- = \begin{pmatrix} \underline{d}_n^{-1} & \underline{d}_n^{-2} \end{pmatrix}, \quad (\text{A13})$$

$$\underline{d}_n^{+1} = \begin{pmatrix} -1 \\ 1 \\ -2 \\ 2 \end{pmatrix}, \quad \underline{d}_n^{+2} = \begin{pmatrix} 1 \\ 1-t_n \\ 2t_n \\ 0 \end{pmatrix}, \quad \underline{d}_n^{-1} = \begin{pmatrix} -1 \\ -1 \\ 2 \\ 2 \end{pmatrix}, \quad \underline{d}_n^{-2} = \begin{pmatrix} 1 \\ -1+t_n \\ -2t_n \\ 0 \end{pmatrix}, \quad (\text{A14})$$

$$\underline{a}_n^{\text{PSV}+} = \begin{pmatrix} a_n^{\text{PSV}+1} \\ a_n^{\text{PSV}+2} \end{pmatrix}, \quad \underline{a}_n^{\text{PSV}-} = \begin{pmatrix} a_n^{\text{PSV}-1} \\ a_n^{\text{PSV}-2} \end{pmatrix}, \quad (\text{A15})$$

and

$$\underline{0}_2 = \begin{pmatrix} 0 & 0 \\ 0 & 0 \end{pmatrix}. \quad (\text{A16})$$

in the bottom layer (i.e. $n = N$), $a_{N+1}^{\text{PSV}+} = a_{N+1}^{\text{PSV}+2} = 0$ to assure the convergence condition at $z \rightarrow \infty$. Note that this is rewritten as

$$\begin{pmatrix} \hat{u}_z^n(z) \\ k^{-1}\hat{u}_V^n(z) \\ G_n^{-1}k^{-1}\hat{t}_{zz}^n(z) \\ G_n^{-1}k^{-2}\hat{t}_{Vz}^n(z) \end{pmatrix} = e^{-k(z-z_{n-1})} \left[a_n^{\text{PSV}+1} \underline{d}_n^{+1} + a_n^{\text{PSV}+2} \underline{d}_n^{+2} \right] + t_n k z e^{-k(z-z_{n-1})} a_n^{\text{PSV}+2} \underline{d}_n^{+1} \\ + e^{-k(z_n-z)} \left[a_n^{\text{PSV}-1} \underline{d}_n^{-1} + a_n^{\text{PSV}-2} \underline{d}_n^{-2} \right] - t_n k z e^{-k(z_n-z)} a_n^{\text{PSV}-2} \underline{d}_n^{-1}. \quad (\text{A17})$$

each component of this is in the same form as eq. (50).

Coefficients $\underline{a}_n^{\text{PSV}+}$ and $\underline{a}_n^{\text{PSV}-}$ are determined by boundary conditions (eqs 48 and 49). The boundary conditions are expressed as

$$\left(\begin{pmatrix} \underline{d}_1^+ \\ \underline{a}_1^{\text{PSV}+} \end{pmatrix}_{\text{lower}} \underline{W}_1^+(z_0) \quad \begin{pmatrix} \underline{d}_1^- \\ \underline{a}_1^{\text{PSV}-} \end{pmatrix}_{\text{lower}} \underline{W}_1^-(z_0) \right) \begin{pmatrix} \underline{a}_1^{\text{PSV}+} \\ \underline{a}_1^{\text{PSV}-} \end{pmatrix} = \begin{pmatrix} 0 \\ 0 \end{pmatrix}, \quad (\text{A18})$$

$$\left(\begin{pmatrix} \underline{d}_n^+ \underline{W}_n^+(z_n) & \underline{d}_n^- \underline{W}_n^-(z_n) & -\underline{C}_{n+1}^{\text{PSV}} \underline{d}_{n+1}^+ \underline{W}_{n+1}^+(z_n) & -\underline{C}_{n+1}^{\text{PSV}} \underline{d}_{n+1}^- \underline{W}_{n+1}^-(z_n) \end{pmatrix} \begin{pmatrix} \underline{a}_n^{\text{PSV}+} \\ \underline{a}_n^{\text{PSV}-} \\ \underline{a}_{n+1}^{\text{PSV}+} \\ \underline{a}_{n+1}^{\text{PSV}-} \end{pmatrix} \right) = -\delta_{sn} \underline{S}^{\text{PSV}}, \quad (1 \leq n \leq N-1) \quad (\text{A19})$$

$$\left(\begin{pmatrix} \underline{d}_N^+ \underline{W}_N^+(z_N) & \underline{d}_N^- \underline{W}_N^-(z_N) & -\underline{C}_{N+1}^{\text{PSV}} \underline{d}_{N+1}^+ \underline{W}_{N+1}^+(z_N) \end{pmatrix} \begin{pmatrix} \underline{a}_N^{\text{PSV}+} \\ \underline{a}_N^{\text{PSV}-} \\ \underline{a}_{N+1}^{\text{PSV}+} \end{pmatrix} \right) = -\delta_{sN} \underline{S}^{\text{PSV}}, \quad (\text{A20})$$

respectively, where

$$\underline{C}_{n+1}^{\text{PSV}} = \begin{pmatrix} \underline{1}_2 & \underline{0}_2 \\ \underline{0}_2 & G_{n+1} G_n^{-1} \underline{1}_2 \end{pmatrix}, \quad (\text{A21})$$

$$\underline{1}_2 = \begin{pmatrix} 1 & 0 \\ 0 & 1 \end{pmatrix}, \quad (\text{A22})$$

where $(\underline{d}_1^+)_{\text{lower}}$ and $(\underline{d}_1^-)_{\text{lower}}$ are the bottom two rows of matrices \underline{d}_1^+ and \underline{d}_1^- , respectively; and $\underline{S}^{\text{PSV}}$ represents the source vectors. Eqs (A18)–(A20) form $4N + 2$ linear algebraic equations so that $4N + 2$ unknown parameters in $\underline{a}_n^{\text{PSV}+}$ ($1 \leq n \leq N + 1$) and $\underline{a}_n^{\text{PSV}-}$ ($1 \leq n \leq N$) are determined for a given $\underline{S}^{\text{PSV}}$.

A.3 Source vectors $\underline{S}^{\text{PSV}}$ and $\underline{S}^{\text{SH}}$

Source vectors $\underline{S}^{\text{PSV}}$ and $\underline{S}^{\text{SH}}$ are defined by using a discontinuity vector (eq. 49 with $n = s$) as

$$\underline{S}^{\text{PSV}} = \left([\hat{u}_z]_s^+, k^{-1} [\hat{u}_V]_s^+, G_s^{-1} k^{-1} [\hat{t}_{zz}]_s^+, G_s^{-1} k^{-2} [\hat{t}_{Vz}]_s^+ \right)^T, \quad (\text{A23})$$

$$\underline{S}^{\text{SH}} = (k^{-1} [\hat{u}_H]_+^+, G_s^{-1} k^{-2} [\hat{v}_{Hz}]_+^+)^T, \quad (\text{A24})$$

where $[f]_+^+$ represents $f(z_s + 0) - f(z_s - 0)$. The explicit forms of these vectors are

$$\begin{aligned} \underline{S}^{\text{PSV}}(m=0) &= (2\pi G_s)^{-1} \left[M_{zz}, 0, 0, \frac{1}{2} (M_{xx} + M_{yy}) - M_{zz} \frac{\lambda_s}{\lambda_s + 2G_s} \right]^T, \\ \underline{S}^{\text{PSV}}(m=\pm 1) &= (2\pi G_s)^{-1} \left[0, \frac{1}{2} (\pm M_{xz} - i M_{yz}), 0, 0 \right]^T, \\ \underline{S}^{\text{PSV}}(m=\pm 2) &= (2\pi G_s)^{-1} \left[0, 0, 0, \frac{1}{4} \{ (M_{yy} - M_{xx}) \pm 2i M_{xy} \} \right]^T, \end{aligned} \quad (\text{A25})$$

$$\underline{S}^{\text{SH}}(m=0) = [0, 0]^T,$$

$$\begin{aligned} \underline{S}^{\text{SH}}(m=\pm 1) &= (2\pi G_s)^{-1} \left[\frac{1}{2} (\pm M_{yz} - i M_{xz}), 0 \right]^T, \\ \underline{S}^{\text{SH}}(m=\pm 2) &= (2\pi G_s)^{-1} \left[0, \frac{1}{4} \{ \pm i (M_{xx} - M_{yy}) + 2M_{xy} \} \right]^T, \end{aligned} \quad (\text{A26})$$

where M_{ij} ($i, j = x, y, z$) is a moment density tensor. The derivation of an equivalent result can be found in chapter 4.4 in Kennett (2009), except for a minor difference owing to the scaling conventions of the Fourier transform. When dislocation on a fault plane is given, the moment density tensor is given by

$$M_{ij} = \lambda_s (v_x U_x + v_y U_y + v_z U_z) \delta_{ij} + G_s (v_i U_j + v_j U_i), \quad (\text{A27})$$

where U_i and v_i ($i = x, y, z$) represent the dislocation vectors of the upper layer and the unit normal to the fault plane, respectively (Aki & Richards 2002).

APPENDIX B: EXPRESSION OF THE MAGNETIC FIELD IN THE WAVENUMBER DOMAIN

The governing equations for \hat{H}_z and \hat{H}_V (eqs 51 and 52) in the n th layer (i.e. $z < z_0$ for $n = 0$, $z_{n-1} < z < z_n$ for $n \leq N$ and $z_N < z$ for $n = N + 1$), denoted by \hat{H}_z^n and \hat{H}_V^n , respectively, are written as

$$\partial_z \hat{H}_z^n(k, m, z) = -kk^{-1} \hat{H}_V^n(k, m, z) - \hat{f}^n(k, m, z),$$

$$\partial_z k^{-1} \hat{H}_V^n(k, m, z) = -k \hat{H}_z^n(k, m, z), \quad (\text{B1})$$

where \hat{f}^n is defined in the n th layer and is expressed in the form of

$$\hat{f}^n(k, m, z) = +\hat{f}_{+1}^n(k, m) e^{-k(z-z_{n-1})} + \hat{f}_{+2}^n(k, m) kze^{-k(z-z_{n-1})} + \hat{f}_{-1}^n(k, m) e^{-k(z_n-z)} + \hat{f}_{-2}^n(k, m) kze^{-k(z_n-z)}. \quad (\text{B2})$$

the boundary conditions of the magnetic field at $z = z_n$ ($0 \leq n \leq N$) are

$$\hat{H}_z^n(z_n) + \hat{m}_z^n(z_n) = \hat{H}_z^{n+1}(z_n) + \hat{m}_z^{n+1}(z_n),$$

$$\hat{H}_V^n(z_n) = \hat{H}_V^{n+1}(z_n). \quad (\text{B3})$$

the magnetization \hat{m}_z^n is expressed in the same form as that of eq. (B2).

A particular solution of this equation is given in the form of

$$\begin{aligned} \hat{H}_z^n = \hat{S}_z^n(k, m, z) \equiv & \hat{S}_{z,+1}^n(k, m) e^{-k(z-z_{n-1})} + \hat{S}_{z,+2}^n(k, m) kze^{-k(z-z_{n-1})} + \hat{S}_{z,+3}^n(k, m) k^2 z^2 e^{-k(z-z_{n-1})} \\ & + \hat{S}_{z,-1}^n(k, m) e^{-k(z_n-z)} + \hat{S}_{z,-2}^n(k, m) kze^{-k(z_n-z)} + \hat{S}_{z,-3}^n(k, m) k^2 z^2 e^{-k(z_n-z)}, \end{aligned} \quad (\text{B4})$$

and the same form for \hat{H}_V^n , with

$$\hat{S}_{z,+1}^n(k, m) = +\frac{1}{2} \hat{f}_{+1}^n(k, m) + \frac{1}{4} \hat{f}_{+2}^n(k, m),$$

$$k^{-1} \hat{S}_{V,+1}^n(k, m) = 0, \quad (\text{B5})$$

$$\hat{S}_{z,+2}^n(k, m) = -\frac{1}{2} \hat{f}_{+1}^n(k, m) + \frac{1}{4} \hat{f}_{+2}^n(k, m),$$

$$k^{-1} \hat{S}_{V,+2}^n(k, m) = -\frac{1}{2} \hat{f}_{+1}^n(k, m) - \frac{1}{4} \hat{f}_{+2}^n(k, m), \quad (\text{B6})$$

$$\begin{aligned} \hat{S}_{z,+3}^n(k, m) &= -\frac{1}{4} \hat{f}_{+2}^n(k, m), \\ k^{-1} \hat{S}_{V,+3}^n(k, m) &= -\frac{1}{4} \hat{f}_{+2}^n(k, m), \end{aligned} \tag{B7}$$

$$\begin{aligned} \hat{S}_{z,-1}^n(k, m) &= -\frac{1}{2} \hat{f}_{-1}^n(k, m) + \frac{1}{4} \hat{f}_{-2}^n(k, m), \\ k^{-1} \hat{S}_{V,-1}^n(k, m) &= 0, \end{aligned} \tag{B8}$$

$$\begin{aligned} \hat{S}_{z,-2}^n(k, m) &= -\frac{1}{2} \hat{f}_{-1}^n(k, m) - \frac{1}{4} \hat{f}_{-2}^n(k, m), \\ k^{-1} \hat{S}_{V,-2}^n(k, m) &= +\frac{1}{2} \hat{f}_{-1}^n(k, m) - \frac{1}{4} \hat{f}_{-2}^n(k, m), \end{aligned} \tag{B9}$$

$$\begin{aligned} \hat{S}_{z,-3}^n(k, m) &= -\frac{1}{4} \hat{f}_{-2}^n(k, m), \\ k^{-1} \hat{S}_{V,-3}^n(k, m) &= \frac{1}{4} \hat{f}_{-2}^n(k, m), \end{aligned} \tag{B10}$$

Using this particular solution, general solutions are expressed in the form

$$\begin{pmatrix} \hat{H}_z^n(z) \\ k^{-1} \hat{H}_V^n(z) \end{pmatrix} = w_n^+(k, m) e^{-k(z-z_{n-1})} \begin{pmatrix} 1 \\ 1 \end{pmatrix} + w_n^-(k, m) e^{-k(z_n-z)} \begin{pmatrix} -1 \\ 1 \end{pmatrix} + \begin{pmatrix} \hat{S}_z^n(z) \\ k^{-1} \hat{S}_V^n(z) \end{pmatrix}, \tag{B11}$$

where w_n^+ and w_n^- ($0 \leq n \leq N + 1$) are integral constants that should be determined by boundary conditions.

Using eq. (B8), the boundary conditions at $z = z_0 = 0$, at $z = z_n$ ($1 \leq n < N$), and at $z = z_N$ are expressed in the forms of

$$\begin{pmatrix} -1 & -1 & e^{-kh_1} \\ 1 & -1 & -e^{-kh_1} \end{pmatrix} \begin{pmatrix} w_0^- \\ w_1^+ \\ w_1^- \end{pmatrix} = \begin{pmatrix} \hat{S}_z^1(z_0) + \hat{m}_z^1(z_0) \\ k^{-1} \hat{S}_V^1(z_0) \end{pmatrix}, \tag{B12}$$

$$\begin{pmatrix} e^{-kh_n} & -1 & -1 & e^{-kh_{n+1}} \\ e^{-kh_n} & 1 & -1 & -e^{-kh_{n+1}} \end{pmatrix} \begin{pmatrix} w_n^+ \\ w_n^- \\ w_{n+1}^+ \\ w_{n+1}^- \end{pmatrix} = \begin{pmatrix} \hat{S}_z^{n+1}(z_n) - \hat{S}_z^n(z_n) + \hat{m}_z^{n+1}(z_n) - \hat{m}_z^n(z_n) \\ k^{-1} \hat{S}_V^{n+1}(z_n) - k^{-1} \hat{S}_V^n(z_n) \end{pmatrix}, \tag{B13}$$

$$\begin{pmatrix} e^{-kh_N} & -1 & -1 \\ e^{-kh_N} & 1 & -1 \end{pmatrix} \begin{pmatrix} w_N^+ \\ w_N^- \\ w_{N+1}^+ \end{pmatrix} = \begin{pmatrix} -\hat{S}_z^N(z_N) - \hat{m}_z^N(z_N) \\ -k^{-1} \hat{S}_V^N(z_N) \end{pmatrix}, \tag{B14}$$

respectively, where $h_n = z_n - z_{n-1}$. Eqs (B12)–(B14) form $2N + 2$ linear algebraic equations so that $2N + 2$ unknown parameters, w_n^+ ($1 \leq n \leq N + 1$) and w_n^- ($1 \leq n \leq N$), are determined for given \hat{S}_z^n and \hat{S}_V^n ($n = 0, \dots, N + 1$).

APPENDIX C: CORRECTION TERMS CORRESPONDING TO SINGULAR POINTS

Below, Cartesian coordinates are adopted. Correction terms appearing in eq. (69) in the main text are expressed in the form of

$$\Delta \mathbf{B}(x, y, z) = \mu_0 \Delta \mathbf{H}(x, y, z) = -\mu_0 \text{grad}(\Delta W(x, y, z)). \tag{C1}$$

The potential $\Delta W(x, y, z)$ is given in the form of

$$\Delta W(x, y, z) = [C_x \Delta w_{ij}^x(x, y, z) + C_y \Delta w_{ij}^y(x, y, z) + C_z \Delta w_{ij}^z(x, y, z)] v_j \Delta u_i, \tag{C2}$$

where Δu_i and v_j are the dislocation vectors of the upper medium and the unit vector direction normal to the fault, respectively, and

$$C_k = \frac{1}{8\pi} \beta M_k G_s \frac{3\lambda_s + 2G_s}{\lambda_s + G_s}, \quad (k = x, y, z) \tag{C3}$$

where s is the source level (Fig. 1).

Each Δw_{ij}^m is given by

$$\begin{aligned} \Delta w_{xx}^x &= 2C_x P \left(-\frac{x}{\rho^3} \right), \\ \Delta w_{xx}^y &= -2C_y Q \left(-\frac{y}{\rho^3} \right), \end{aligned}$$

$$\Delta w_{xx}^z = -2C_z(P - Q) \left[-\frac{z - z_s}{\rho^3} \right], \quad (C4)$$

$$\Delta w_{yy}^x = -2C_x Q \left(-\frac{x}{\rho^3} \right),$$

$$\Delta w_{yy}^y = 2C_y P \left(-\frac{y}{\rho^3} \right),$$

$$\Delta w_{yy}^z = -2C_z(P - Q) \left[-\frac{z - z_s}{\rho^3} \right], \quad (C5)$$

$$\Delta w_{xy}^x = \Delta w_{yx}^x = C_x(P + Q) \left(-\frac{y}{\rho^3} \right),$$

$$\Delta w_{xy}^y = \Delta w_{yx}^y = C_y(P + Q) \left(-\frac{x}{\rho^3} \right),$$

$$\Delta w_{xy}^z = \Delta w_{yx}^z = 0, \quad (C6)$$

and

$$\Delta w_{iz}^k = \Delta w_{zi}^k = 0, \quad (i, k = x, y, z) \quad (C7)$$

where

$$P = \frac{\alpha(1 + 2\alpha)}{4\alpha - 1}, \quad Q = \frac{2\alpha(1 - \alpha)}{4\alpha - 1},$$

$$\alpha = \frac{\lambda_s + G_s}{\lambda_s + 2G_s}, \quad (C8)$$

and where

$$\rho = \sqrt{x^2 + y^2 + (z - z_s)^2}. \quad (C9)$$

These results are derived from the discussion in section 5.2 of Sasai (1991a), as explicitly given in eqs (5.24)–(5.29) with eq. (4.17) and the definition of $w_{ij}^{m(P)}$ in the following page of his paper. Note that there is a difference of factor 4π between eq. (C3) and eq. (4.17) of Sasai (1991a), which originates from the difference in the system of units adopted in the two papers.

APPENDIX D: COMPARISON WITH RIGOROUS SOLUTIONS

This appendix is provided to demonstrate that the displacement and piezomagnetic fields corresponding to uniform slip on a rectangular fault are determined by the presented procedure, namely, dividing the rectangular fault into small subfaults and approximating them by points, with sufficient accuracy for the discussion in the main text. The evaluation is performed through a comparison between calculated values with analytical solutions that have already been tested and those of the present procedure. Although the comparison can be conducted only for the case of uniform rigidity, the sufficiency of the subfault size can be evaluated by this test.

In Figs D1–D3, numerical values determined by the present procedure are compared with those determined by analytical formulae for strike-slip, dip-slip, and tensile-opening, respectively. In the present procedure, a rectangular fault is divided into multiple subfaults, and each subfault is approximated by a point source at its centroid. Sizes of subfaults are set as described in the main text. Analytical formulae of the piezomagnetic field have been presented by Sasai (1991a) and Utsugi *et al.* (2000) and of the displacement field have been presented by Okada (1992). Fortran programs provided by M. Utsugi and Y. Okada were used for these analytical formulae. When using Utsugi's programme, a condition of $z = -1$ m (above ground level) is assumed, whereas a condition of $z = +1$ m (below ground level) is assumed in the present procedure. This is because the solution of Utsugi *et al.* is derived for $z < 0$, although his code accepts a positive value of z . Because values of ΔF calculated using eqs (70) and (71) are continuous at ground level ($z = 0$), this comparison is meaningful regardless of the small difference in z . In calculating the piezomagnetic field for strike-slip and tensile-opening models, results corresponding to dip angles of $90^\circ \pm 1^\circ$ are averaged to obtain a result for a vertical fault because the program provided by M. Utsugi cannot be applied to the fault with a dip angle of 90° .

The comparison shows that the difference appears only near the fault and is up to 20 per cent of the maximum variation in each component, meaning that the numerical results are sufficiently accurate for discussion in the main text, in which only differences larger than 20 per cent are considered. Note that a finer division of the rectangle will be required when the observation is conducted near the dislocation source because the point approximation is valid only when the size of the dislocation source is smaller than the distance between the source and the observation point. For this reason, validation of accuracy should be performed when considering a model with a different configuration.

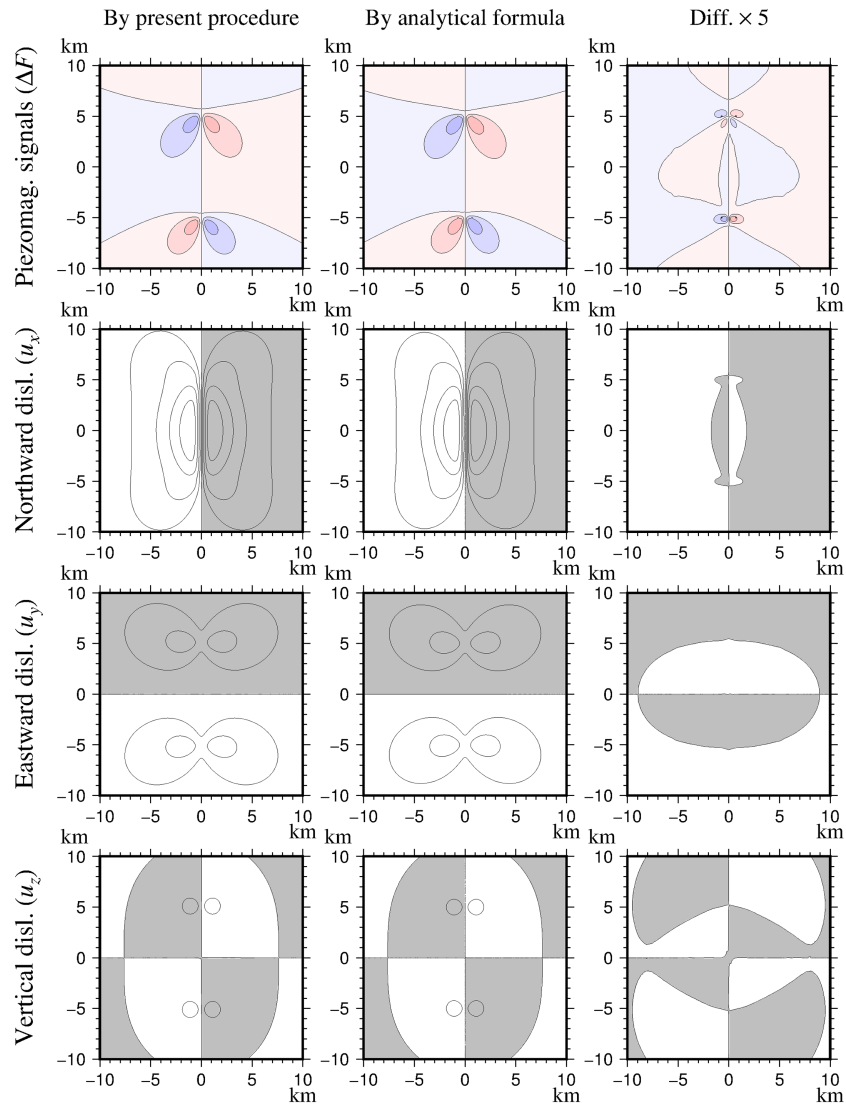


Figure D1. Comparison of values calculated using the present procedure (left panel) and using analytical formula (center panel) for a strike-slip model, together with their differences (right panel). The left and center panels are drawn using the same colors and contour intervals as those of Figs 5 and 7–11. Values in the right panel are multiplied by 5.

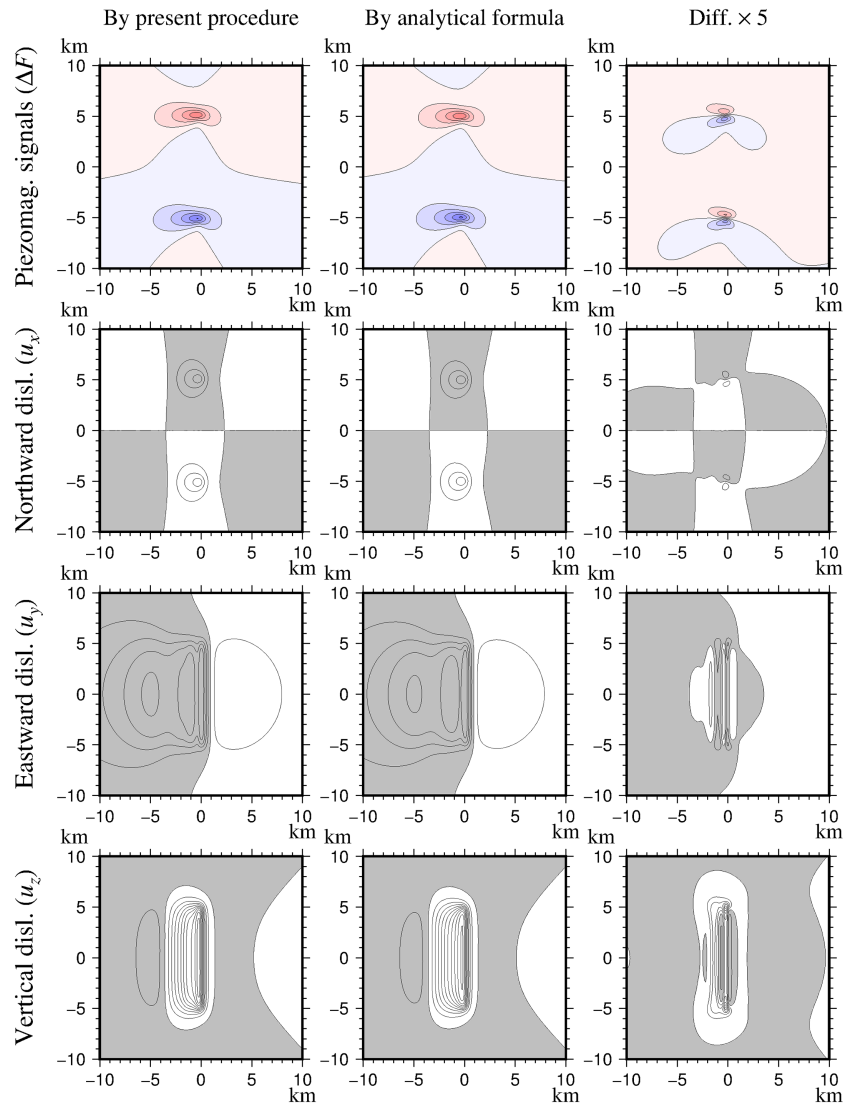


Figure D2. Comparison of values calculated using the present procedure and using analytical formula for a dip-slip model, drawn in the same manner as Fig. D1.

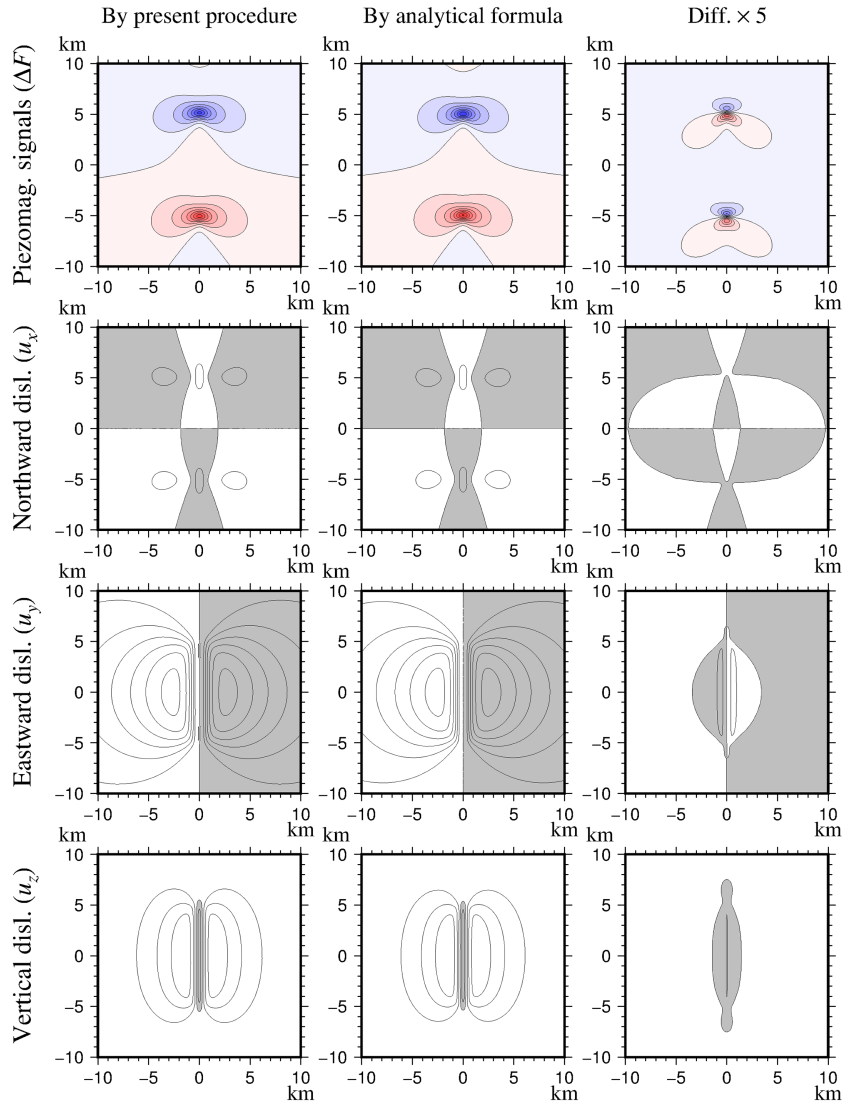


Figure D3. Comparison of values calculated using the present procedure and using analytical formula for a tensile-open model drawn in the same manner as Figs D1 and D2.